WL-TR-97-2093

CRYO POWER AND HEAT TRANSFER

L. CHOW
C. GU
W. LU
R. MAURIELLO
D. NGUYEN

UNIVERSITY OF CENTRAL FLORIDA
DEPARTMENT OF MECHANICAL, MATERIALS AND AEROSPACE
        ENGINEERING
ORLANDO, FLORIDA 32816-2450

AUGUST, 1997

INTERIM REPORT FOR 07/17/96 - 07/31/97

|DTIC QUALITY INSPECTED 3

19980415 164

NOTICE

USING GOVERNMENT DRAWINGS, SPECIFICATIONS, OR OTHER DATA INCLUDED IN THIS DOCUMENT FOR ANY PURPOSE OTHER THAN GOVERNMENT PROCUREMENT DOES NOT IN ANY WAY OBLIGATE THE US GOVERNMENT. THE FACT THAT THE GOVERNMENT FORMULATED OR SUPPLIED THE DRAWINGS, SPECIFICATIONS, OR OTHER DATA DOES NOT LICENSE THE HOLDER OR ANY OTHER PERSON OR CORPORATION; OR CONVEY ANY RIGHTS OR PERMISSION TO MANUFACTURE, USE, OR SELL ANY PATENTED INVENTION THAT MAY RELATE TO THEM.

THIS REPORT IS RELEASABLE TO THE NATIONAL TECHNICAL INFORMATION SERVICE (NTIS). AT NTIS, IT WILL BE AVAILABLE TO THE GENERAL PUBLIC, INCLUDING FOREIGN NATIONS.

THIS TECHNICAL REPORT HAS BEEN REVIEWED AND IS APPROVED FOR PUBLICATION.

BRIAN D. DONOVAN
Project Engineer
Mechanical Branch
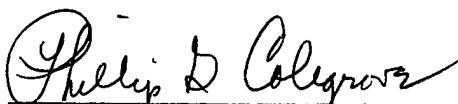
PHILLIP G. COLEGROVE
Chief, Mechanical Branch
Power Division

MICHAEL D. BRAYDICH, LT COL, USAF
Chief
Power Division

IF YOUR ADDRESS HAS CHANGED, IF YOU WISH TO BE REMOVED FROM OUR MAILING LIST, OR IF THE ADDRESSEE IS NO LONGER EMPLOYED BY YOUR ORGANIZATION PLEASE NOTIFY WL/POOS. __WRIGHT-PATTERSON AFB OH 45433 -7251_ TO HELP MAINTAIN A CURRENT MAILING LIST.

Do not return copies of this report unless contractual obligations or notice on a specific document requires its return.

REPORT DOCUMENTATION PAGE

1. AGENCY USE ONLY *(Leave blank)*	2. REPORT DATE August 1997	3. REPORT TYPE AND DATES COVERED INTERIM 07/17/96 – 07/31/97

4. TITLE AND SUBTITLE

Cryo Power and Heat Transfer

5. FUNDING NUMBERS

C F33615-96-C-2681
PE 62173C
PR 1651
TA 01
WU 06

6. AUTHOR(S)

L.C.Chow   C.B.Gu   W.F.Lu
R.J.Mauriello   D.D.Nguyen

7. PERFORMING ORGANIZATION NAME(S) AND ADDRESS(ES)

University of Central Florida
Mechanical, Materials and Aerospace Engineering
Orlando, FL 32816-2450

8. PERFORMING ORGANIZATION REPORT NUMBER

9. SPONSORING/MONITORING AGENCY NAME(S) AND ADDRESS(ES)

Aero Propulsion and Power Directorate
Wright Laboratory
Air Force Materiel Command
Wright Patterson AFB, OH 45433-7251
POC: Brian Donovan, WL/POOS   (937) 255-6241

10. SPONSORING/MONITORING AGENCY REPORT NUMBER

WL-TR-97-2093

11. SUPPLEMENTARY NOTES

12a. DISTRIBUTION/AVAILABILITY STATEMENT

Approved for public release; distribution is unlimited

12b. DISTRIBUTION CODE

13. ABSTRACT *(Maximum 200 words)*

The numerous advantages of operating electronics at the cryogenic temperature have made this research increasingly important. Because the foremost problem in electronic cooling is achieving high heat removal capacity within small packages, one focus of this study is to investigate the heat transfer characteristics of various cooling techniques. Pool boiling experiment studies the effects of heater angle orientation and confined spacing on CHF (Critical Heat Flux). The horizontal upward-facing heater gives the highest CHF while the downward-facing position causes significant drop in CHF. The study also finds a critical value (s=2.5 mm) for the confined spacing situation. For the heaters in an array, at the vertical orientation, the influence from the lower heater causes a lower CHF of the higher heater. Forced convective boiling in this study can achieve 4 to 5 times higher heat removal rates than those of pool boiling. A model to describe the heat transfer mechanism near CHF is developed. It is demonstrated that the macrolayer thickness plays the most important role in determining CHF. The effect of flow channel height and heater geometry have been investigated. A practical guideline for the design of a flow boiling system is proposed. A MOSFET (Metal Oxide Semiconductor Field Effect Transistor) will be manufactured, simulated and tested at both room temperature and cryogenic temperature. The simulation results will be compared with the measurements of the real device.

14. SUBJECT TERMS

Cryogens, immersion boiling, convective boiling, power MOSFETs low-temperature electronics, device simulation

15. NUMBER OF PAGES
73

16. PRICE CODE

17. SECURITY CLASSIFICATION OF REPORT	18. SECURITY CLASSIFICATION OF THIS PAGE	19. SECURITY CLASSIFICATION OF ABSTRACT	20. LIMITATION OF ABSTRACT
Unclassified	Unclassified	Unclassified	

TABLE OF CONTENTS

LIST OF FIGURES

NOMENCLATURE

A	area
A_v	vapor column area of a unit boiling cell
A_w	area of a unit heated surface
CHF	critical heat flux, W/cm^2s
D_H	hydraulic diameter based on wetted perimeter
D_0, D_1, D_2	diffusion coefficient
h_{fg}	latent heat of vaporization
H	flow channel height
g	gravitational constant
k	thermal conductivity
LN2	liquid nitrogen
N	concentration of the silicon wafer, cm^{-3}
q''	heat flux, W/cm^2s
q''_c, q''_{CHF}	same as CHF
Re	Reynolds number
s	spacing, mm
T_w, T_{wall}	surface temperature of heater, K
T_{sat}, T_{LN2}	saturation temperature of liquid, K
u	flow velocity
u^+	dimensionless velocity
We	Weber number
x	predep (m)
y^+	dimensionless wall coordinate
z	net profile at junction depth, cm
ΔT	$T_w - T_{sat}$, K
θ	heater orientation, degree

1. INTRODUCTION

The future of high temperature superconductors (HTS) and low temperature MOSFETs (metal-oxide-semiconductor field effect transistors) electronics holds a great deal of promise. The numerous benefits of operating electronics at low temperature have been realized. For one, the circuits operates faster, semiconductors switch more rapidly and the number of thermally-induced device failure decrease. Also the noise-to-signal ratios drop. These advantages are usually associated with operating temperatures between 10 K through 100 K. It is also in this range that the thermal and electrical conductivities of common circuits materials, such as copper and silicon, are maximized. Liquid nitrogen (LN2) is a relatively inexpensive and dielectric cryogenic coolant whose boiling point (77.3 K at 1 atm) falls into this temperature range. In some cases, when the cryogen is used as the heat transfer fluid, the size and weight of the onboard electronics can be reduced by an order of magnitude. However, the successful application of the cryogenic cooling to electronics requires that the appropriate heat transfer characteristics be know.

The primal thermal management techniques for low temperature operations are pool boiling (immersion cooling), forced convective boiling (or flow boiling), spray cooling and jet impingement cooling. This report is the first annual report for the contract F33615-96-C-2681. It focuses on heat transfer issues in pool and flow boiling of power MOSFETs.

Pool boiling in LN2 has a reasonable maximum heat flux removal capacity. It is the easiest to apply in electronic cooling. Although extensive studies have been conducted on pool boiling, they have mostly involved research in conventional pool boiling; i.e., single heat transfer surface in an open pool of liquid. However, the situation in most electronic equipment consists of a series of discrete heat sources that are installed next to one another. The spacing between them is confined. The orientation and space limitation of the chips have been speculated to affect the boiling phenomena significantly. These geometrical factors have been studied in this project.

Flow boiling from an array of discrete heat sources in LN2 has seldom been attempted before. This type of cooling technique involves forced flow of a cryogen. It can remarkably

increase the CHF (critical heat flux) value compared to pool boiling. Experiments have been conducted under various liquid flow velocities to measure the CHF and heat transfer coefficient. Geometrical effects such as flow channel height, heated surface distance and dimension are also studied. A semi-empirical flow boiling model for predicting CHF and macrolayer thickness is presented. Estimation of macrolayer thickness is deemed as the most important aspect of flow boiling analysis. The results of the experiments should provide invaluable guideline for the electronic industry in terms of how compact electronic devices can be packaged without sacrificing the phase-change heat transfer benefit.

Another objective of this project is to fabricate a power MOSFET in the laboratory and perform testing on it at LN2 temperatures, and comparing the results to those obtained at room temperature. Modeling of the temperature effect on MOSFET operation will conducted. A simulation of the MOSFET device using ISE-TACD software is developed and the simulation results will be compared to that of the real device previous fabricated and tested.

2. EFFECTS OF ORIENTATION AND CONFINEMENT ON POOL BOILING OF HEATER SURFACES

2.1 Introduction

This chapter reports the research that has been performed during the first year of the 5 year project funded by Wright Laboratory, Wright-Patterson AFB. It concerns the effects of the orientation, confinement and the array of heated surfaces on the critical heat flux (CHF) from the surfaces. CHF represents the maximum heat transfer rate obtainable through nucleate boiling under given conditions. When the surface temperature is increased above the saturation temperature (the temperature difference is called superheat) of the cooling liquid, nucleation of vapor bubbles begins. As the superheat is increased, more nucleating bubbles appear and grow in size (while merging may well occur). During the nucleate boiling, the liquid is able to replenish the surface when the larger bubbles depart from the surface. As the superheat is further increased, the bubbles depart at a rate higher than the replenishing liquid arriving at the surface. CHF results when the liquid replenishes the surface at a rate just sufficient to be vaporized. At CHF, the surface temperature increases dramatically.

One advantage of using boiling heat transfer is that the temperature of the heated surface can be stabilized within a narrow range of the boiling temperature of liquid used (liquid nitrogen in this study). The performance of the electronic device would likewise be stabilized and predictable. The results should find applications in power electronics and thermal management systems in space.

Many functions performed in high performance electronics can be done by superconductor circuits [1]. Typical high temperature superconductors operate under cryogenic temperatures. Superconductor circuits usually cannot handle high power levels at which the desirable characteristics of superconductors suffer. In the cases of high power electronics silicon-based devices, such as MOSFETs which are used in conjunction with superconductors; one obtains what

are referred to as semiconductor hybrid circuits. At low temperatures the resistance of MOSFETs can drop by a factor of 10-15 at low drain currents and by a factor of 25-30 at the rated drain current compared to room temperature operation [2]. Superconductor and its hybrid circuits have found many other applications such as magnets used in nuclear particle accelerators, superconducting gates, digital logic and memory devices, high-speed analog-to-digital converters, and high-speed computers. As the performance requirements increase, the energy dissipation rate in these devices increases, resulting in an increase in resistance and limitations on further improvement. It is then desirable to cool superconductor circuits at cryogenic temperatures of such fluids as LN2. The latent heat associated with the phase change suits the high power dissipation rates in these circuits and devices. Overall operation at low temperatures has the following advantages: faster circuits, more rapid semiconductor switching, reduction in thermally-induced failures and increased signal-to-noise ratio.

LN2 is a relatively inexpensive coolant whose boiling temperature (77.3 K at 1 atm) falls into the desirable temperature range. Other cryogens often have undesirable characteristics such as toxicity (CO), corrosiveness (F_2), and fire hazards (H_2, O_2). LN2 has been used in practice and research in electronic device cooling [3-5]. Most of these studies concentrated on pool or flow/convective boiling of LN2, while others on spray cooling. In practice, spray cooling may not be possible as in the case of closely spaced circuit boards. Frequently the circuit boards may not be horizontally oriented and the results from many pool boiling studies are not directly applicable. It is known that buoyancy plays an important role in determining the values of CHF while the heater surface orientation is varied [6]. This is attributed to the change in the pattern of the vapor bubble departing the heater surface. When the heater is vertically positioned, bubbles depart the lower surface and hence induce flow over the upper part of the heater surface. However, in the absence of strong forced convection, the induced flow may not be able to remove the vapor bubble from the upper part of the heater surface. Combining with the lack of the gravitational action normal to and away from the heater surface, the vertically positioned heater is expected to have lower CHF compared to the upward-facing heaters. This effect of heater orientation is most significant when bulk fluid is at rest [6], i.e., pool boiling. Furthermore, the CHF is expected to be lowered when the heater surface faces downward because the vapor bubble cannot depart as in

4

upward-facing position. It then presses against the heater, preventing the liquid from wetting the surface and dryout occurs.

Compact designs of circuit boards are desirable, especially for space applications, where circuit boards are expected to be closely spaced. Small spacing will certainly affect/impede the departure of the nucleating vapor bubbles, resulting in the onset of dryout and lowering CHFs. This effect should be acute when the spacing is on the same order of bubble size at departure. It is expected that the confinement effects will be further complicated by the heater orientation.

The experiment was designed and the study was conducted with a systematically chosen combination orientation with and without confinement. Results are presented and discussed, followed by a conclusion.

2.2 Research Objectives

The objectives of this study are to quantify the effects of the following on the heat transfer characteristics and CHF in liquid nitrogen (LN2) pool boiling: (1) heater orientation, (2) heater confinement , and (3) the combination of heater orientation and confinement. The experimental data will be analyzed and its implications discussed. Possible mechanisms for the observed results will also be proposed as will further studies.

2.3 Experimental Setup And Procedure

2.3.1 Experimental Goals

To achieve the research objectives outlined above in an efficient and accurate manner, the following were done:

(1) The experimental apparatus should be able to handle the cryogenic conditions and heat transfer/loss from the test chamber should be minimized.

(2) Data acquisition should be fully computer-assisted to assure consistency and repeatability.

(3) A heater array should be used so that the effects of vapor bubbles generated at the lower heater on the heat transfer characteristics of the upper heater can be studied.

(4) Heater orientation should be easily achieved and confinement should be easily attachable to and detachable from the heater array.

2.3.2 Experimental Design

Figure 2.1 is a schematic view of the experimental setup. It consisted of six parts, as indicated by Roman numerals in the figure. Part I, called the experimental chamber, is the core of the experiment and includes a beaker (which contained LN2 during the experiment), a heater stand, and a heater module/array (3 x 3, shown in Figure 2.2 below). The beaker, made of Pyrex glass, is 15 cm in inside diameter and approximately 18 cm in depth. The LN2 level allowed the total immersion of the heater array. The protractor, marked for every 10°, was attached to a rotating mechanism that allowed the rotation of the heater module. The axis of rotation passed through midway between the shorter sides of the rectangular heater module. Part I was placed inside the middle chamber (designated as Part II in Figure 2.1; Plexiglas, having a 19 cm inside diameter and a 0.5 cm thickness), which in turn was placed inside the outside chamber (Part III in Figure 2.1; Plexiglas, having a 23.5 cm inside diameter and a 0.94 cm thickness). The space between the middle and outer chambers was vacuumed and served as the insulator that shields the LN2 from the room temperature. The space between the beaker and the middle chamber was intended to provide further insulation so that possible radiation heat transfer to the beaker wall will be minimized. This further insulation was necessary if visualization was to be accomplished on the nucleation phenomena of the heater surface. In fact, the vacuum serves similar purposes because the room air will not be in direct contact with the cold inside chamber to result in condensation of moisture in the laboratory and prevent visualization.
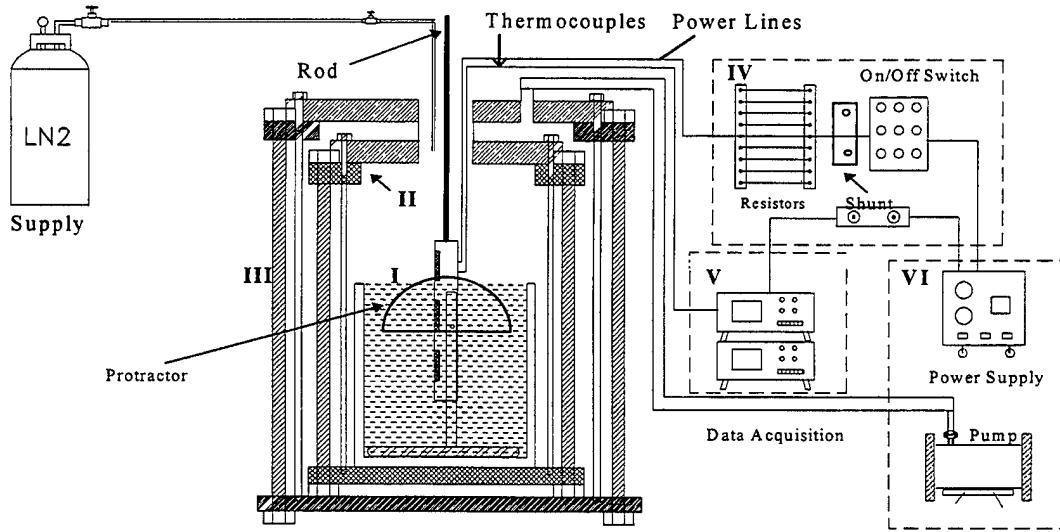
Figure 2.1   Experimental Set-up
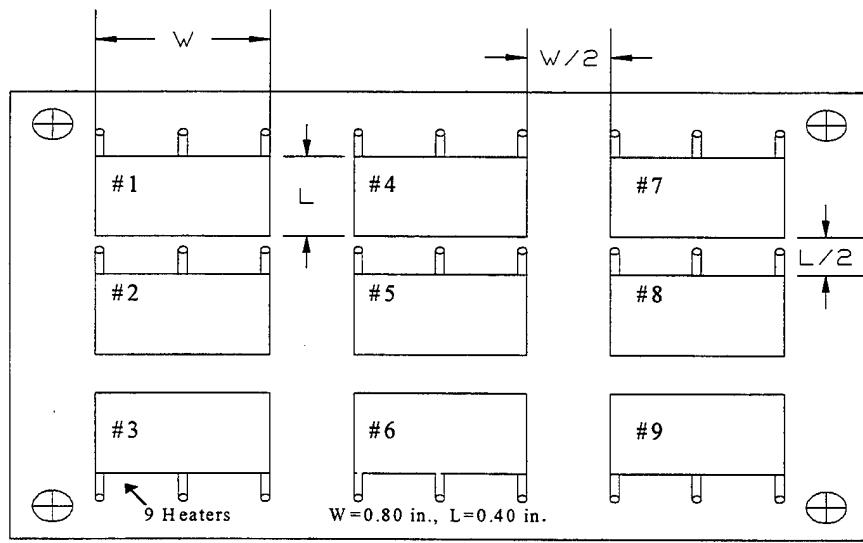
Figure 2.2   Heater Module

The heater module is an acrylic block that serves as the base for the nine heaters as well as an insulator between them. Each heater, made from copper, is rectangular in shape and has the dimensions of 2.0 cm x 1.0 cm x 0.25 cm, as shown in Figure 2.2. The nine heaters were flush-mounted to the heater module. Before mounting, packaging was done to include a thermocouple (type E) for heater temperature measurement and a heating element. The thermocouple was inserted through a hole located about 1 mm beneath the center of the upper surface of the copper block; its bead was glued to the copper interior using OmegaBond Epoxy. The detail heater

structure is shown in Figure 2.3. The heating of the copper was achieved by a thin nickel-chromium resistor film that was coated to a ceramic substrate using a chemical vapor deposition technique. The other side of the ceramic substrate was glued to the bottom of the copper block, also by OmegaBond Epoxy. Both the ceramic substrate and the Epoxy have high thermal conductivity. The downward-facing side of the thin film heater was insulated using a silicon sealant. The silicon sealant was also used to fill up gaps and grooves between the heater and the acrylic heater module. As a result, the heat transfer was directed from the thin resistor film to the upper copper surface, which was exposed to LN2 during the experiment, with negligible heat loss to all other sides of the heater.
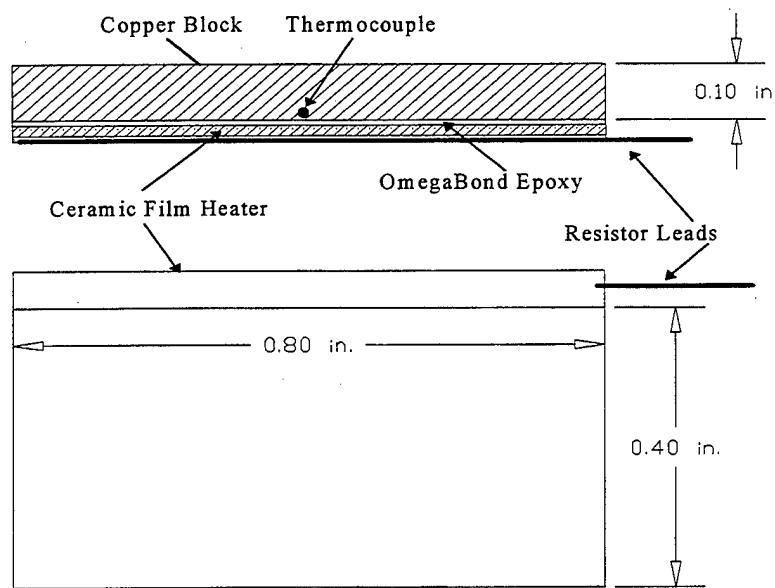
Figure 2.3   Detail Heater Construction

The electric circuits for supplying power to the heater is sketched in Figure 2.1 and was designated as Part IV. Nine heaters were assembled in parallel. Since the resistances were not perfectly equal, an array of nine resistors was designed and connected in series with each heater so that the heat dissipation rates (equal to I^2R, I and R being the current and voltage drop across the heater, respectively) were equal in each of the nine heaters (i.e., the heat transfer rates from the copper surface to LN2 were equal). Detail design of the resistor array was described in Ref. 7.[7]

8

2.3.3 Data Acquisition and Analysis

A Keithley 7001 switch system, Keithley 200 $6^1/2$-digit high performance digital multimeter, and a multichannel thermocouple card were used as the data acquisition system (Part V in Figure 2.1). The system gathered the information for determining heater surface temperature and energy dissipation rate due to the electric current in the heaters. This raw data was fed to and recorded by a computer that also controlled the increase of electric currents as a function of time. Each set of heat transfer rates was determined when the computer detected steady state temperature signals after each increment. This allowed the conventional way of plotting the heat transfer rate from the copper heater surface to the liquid against the superheat (ΔT, defined as the heater surface temperature minus the saturation temperature of the liquid, $T_w - T_{sat}$). The heat transfer coefficient, $h = q'' / \Delta T$, can then be calculated.

Three categories of experiments were conducted to achieved the objectives outlined in Section 2.2. First, data was acquired for seven orientations ($0°$, $30°$, $60°$, $90°$, $180°$, $-30°$, and $-60°$, shown in Figure 2.4) when a single heater was operated. Secondly, a confining flat plate was placed in front of the heater module with four different spacings (3.0, 2.5, 1.5, 0.75 mm) for these seven orientations. The third type of experiments involved determining the heat transfer characteristics of a single top heater (heater no. 9 in Figure 2.2) operating alone and while it operated with lower heaters turned on with the same heat transfer rate. For this third category three orientations were chosen ($0°$, $90°$, and $180°$).

Experimentally, CHF was sighted when there was an excursion in ΔT (= $T_w - T_{sat}$, where the subscript w denotes the heater surface and sat, the boiling/saturation temperature of the liquid) without increase in q''. This is because the liquid could not replenish the heater surface to keep up with the rapid evaporation. The data taking procedure was then terminated and the last heat flux (heat transfer per unit area of the heater surface and per unit time) recorded was the critical heat flux (CHF, or q_c'').

9
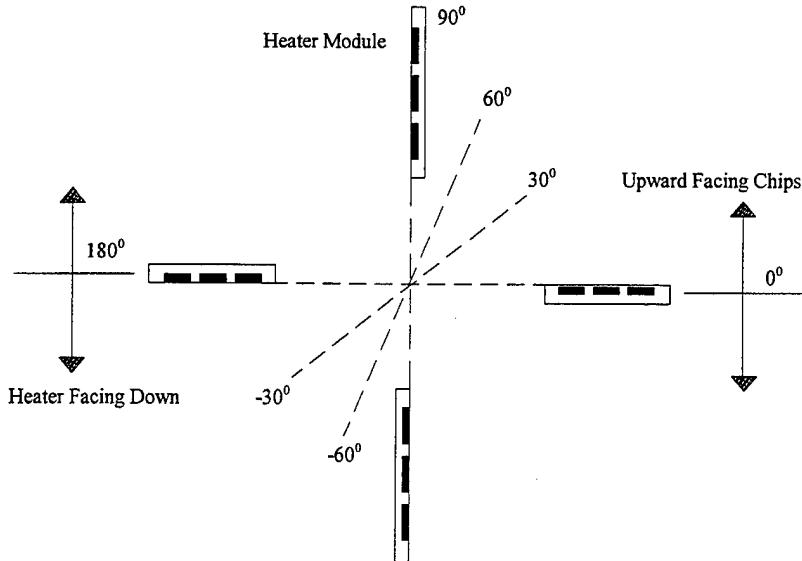
Figure 2.4   Heater Orientation Definition (Diane's thesis figure 3.6)

2.4 Results And Discussion

2.4.1 Effects of Heater Orientation

Results of heat transfer curve as a function of heater superheat without confinement (i.e., open pool boiling) are presented in Figures 2.5 through 2.8. Figure 2.5 shows the results of $\theta = 0^\circ$ (upward-facing), 90° (vertical), and 180° (downward-facing). These are the limiting cases where the values of CHF differ the most. The heat transfer curves of the three heater orientations are typical of pool boiling. The value of ΔT ($\approx 19K$) for CHF at $\theta = 0^\circ$ is similar to previously published results [Sehmey et al., 1995], while the value of CHF (≈ 21 W/cm^2) at $\theta = 90^\circ$ agrees very well with that found by Chui et al. (1995). The values of CHF for $\theta = 0^\circ$, 90°, and 180° are 26.7, 21.2, and 9.4 W/cm^2, respectively. The higher CHF of the horizontal, upward-facing heater is due to the vapor bubbles departing at the heater surface as a result of buoyancy force. Once the bubble departs, liquid will find its way to reach the heater surface to complete the replenishing action. The bubbles at the surface of the downward-facing heater are pressed against it also due to the buoyancy. In this case the vapor accumulates to form bigger bubbles preventing the liquid from replenishing at the surface. The dryout and CHF therefore occurs at a lower superheat. The CHF of the downward-facing heater is approximately 1/3 of that of the upward-facing heater.

10
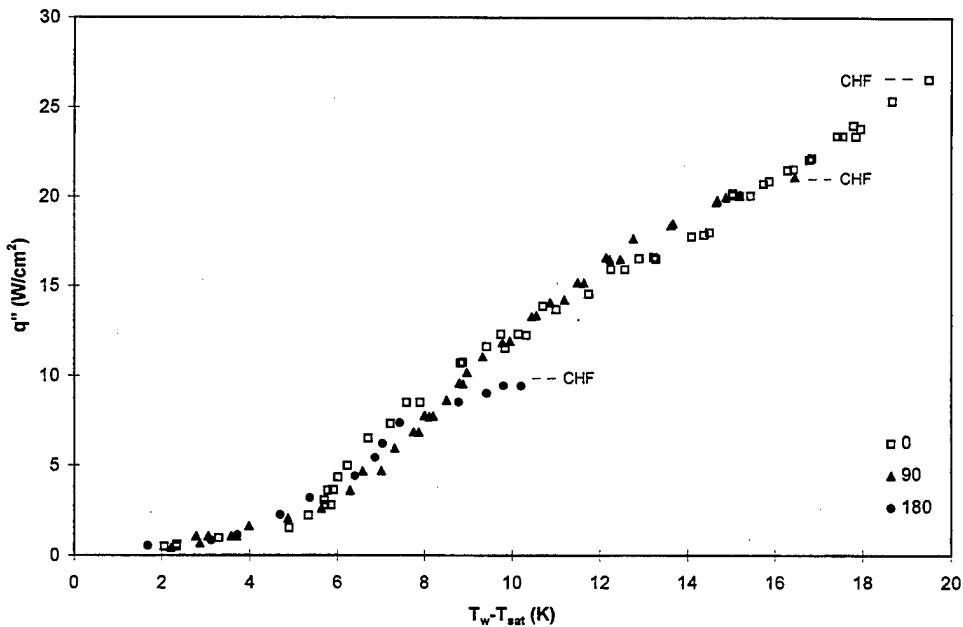
Figure 2.5   Open pool boiling for 0°, 90° and 180°

In Figure 2.6 the heat transfer characteristics and CHF with θ = 30° are compared with those of θ = 0°. The difference in CHF is approximately 10%, with θ = 30° having slightly lower values of CHF (23.7 vs. 26.7 W/cm^2) superheat for CHF (ΔT ≈ 17.8K vs. 18.7K). However, the values of h appear to be the same over most of the entire superheat range. The slight inclination of the heater therefore does not appear to significantly affect the open pool boiling heat transfer and or impede the vapor bubble departure from the heater surface and the liquid replenishing action.

The results of θ = 60°, 90°, and -60° are shown in Figure 2.7. The CHFs (21.5, 20.5, and 19.1 W/cm^2, respectively for θ = 60°, 90°, and -60°) are lower than those of θ = 0° and 30° (26.7 and 23.7 W/cm^2, respectively). The superheat for CHF also decreases as the heater is rotated to a vertical and then to a downward facing positions. This is the continued trend seen in Figure 2.5. As q is increased, the favorable buoyancy factor decreases and the tendency for the vapor bubble to depart from the heater surface also decreases. Dryout then occurs at a lower superheat with a lower CHF.

11
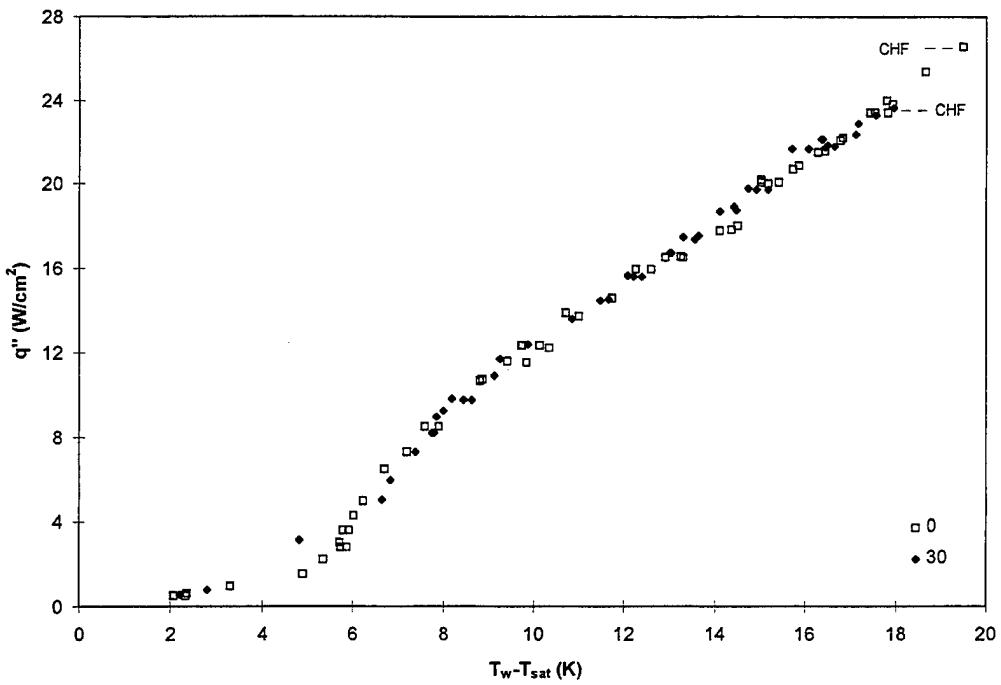
Figure 2.6   Open pool boiling for 0° and 30°

At the same angle from the horizontal plane, the upward-facing heater produces a higher CHF at a larger superheat than the downward-facing heater (e.g., θ = ±60 °, in Figure 2.7). For upward-facing heaters, the buoyancy force acts to press the vapor bubbles against the heater surface and to prevent the bubble departure . Although the slight inclination still allows the vapor bubbles to slide along the heater surface and eventually escape from its edge, it nevertheless takes a longer time for bubble departure than in any upward-facing positions. This means that the liquid cannot replenish the heater surface with as fast a rate as for the upward-facing heater, resulting in dryout at a lower superheat and thus a lower CHF. As the heater is rotated to θ = -30° and 180°, the unfavorable buoyancy action becomes more significant, as can be seen from Figure 2.8. The values of CHFs and superheats at which CHFs occur are further decreased from those of θ = -60°. The change of CHF from θ = -30° to 180° is rather dramatic compared to other 30° changes in orientation, with a 75% decrease as opposed to approximately 10% in other cases (cf. Figures 2.6 and 2.7). The effects of heater orientation are closely related to the action of the buoyancy force. This is best illustrated by θ = 0°, with CHF ≈ 26.7 W/cm² at ΔT ≈ 18K, and 180°, with CHF ≈ 9.5 W/cm² at ΔT ≈ 10K.
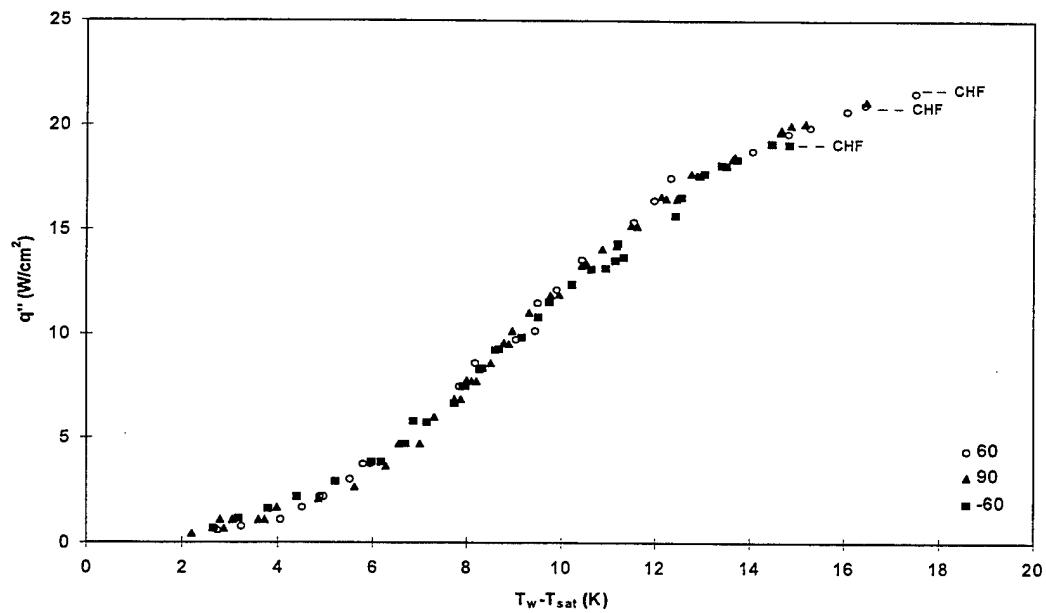
Figure 2.7   Open pool boiling for 60°, 90° and -60°
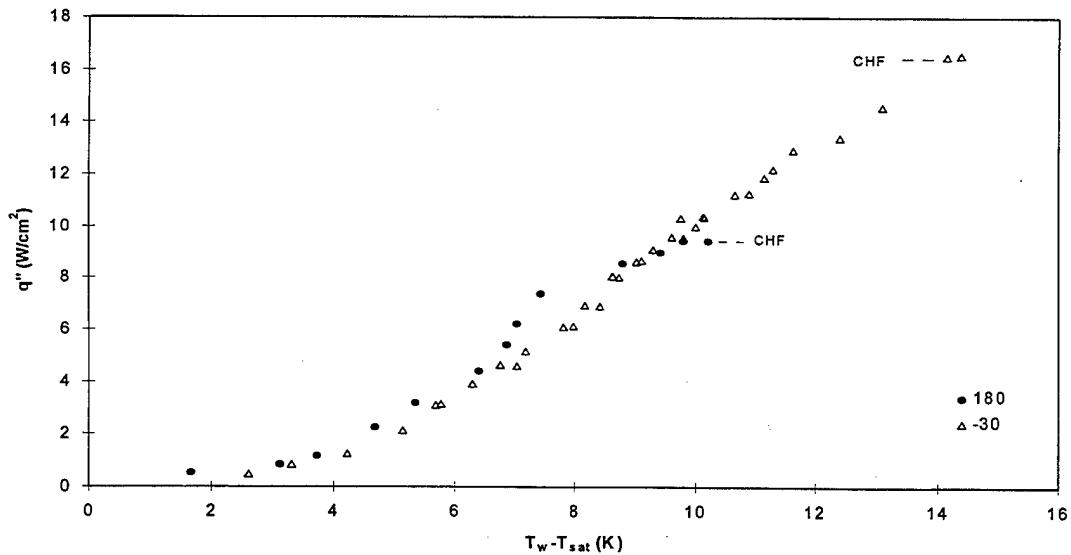
Figure 2.8   Open pool boiling for -30° and 180°

2.4.2 Effects of Confinement

Effects of confinement for $\theta = 0°$, $90°$, and $180°$ can be seen in Figures 2.9 - 2.12. It is noted that with the confinement, $\theta = 90°$ is the only orientation allowing efficient escape of vapor

13

bubbles from the heater and, thus, most rapid liquid replenishing to rewet the heater surface. For θ = 0°, vapor bubbles accumulate and grow in size at the surface of the confining plate. With the decrease of the size of the gap(s), the degree with which bubbles press against the heater surface increases. The pressing effects are enhanced for θ = 180° due to the action of the buoyancy force. Therefore, the values of CHF and the superheat for CHF for the horizontally downward-facing heater are expected to be the smallest considering the direction of the buoyancy force.
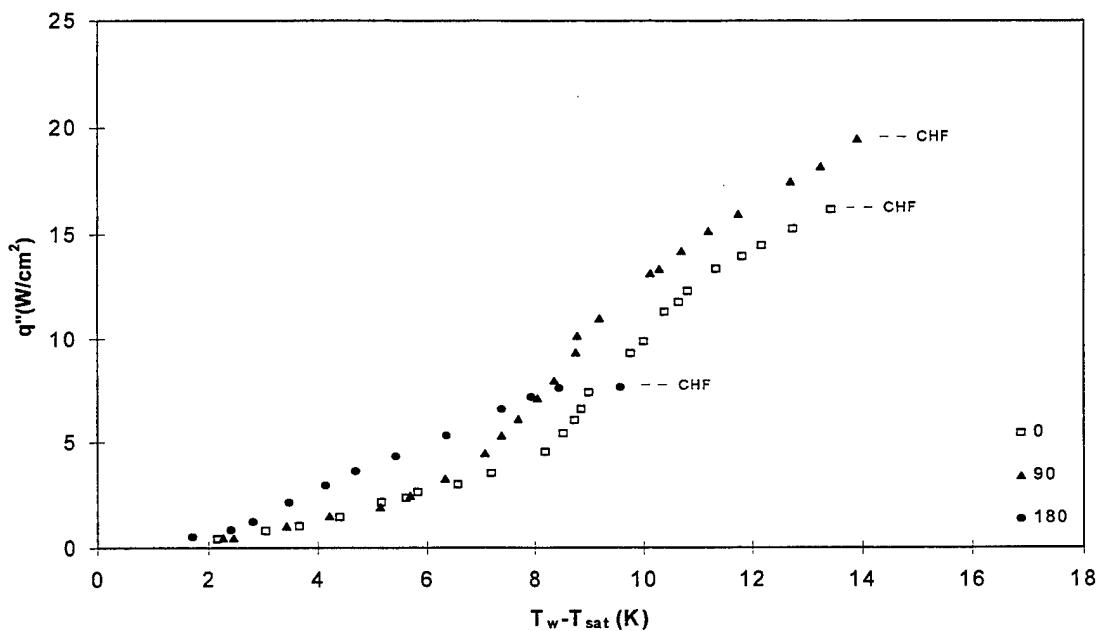
Figure 2.9   Heat transfer characteristics for s=3.0 mm

The values of CHF should therefore decrease in the order of θ = 90°, 0°, and 180°. This is clearly seen in Figures 2.9 - 2.12 for heater spacing(s) = 3.0, 2.5, 1.5 and 0.75 mm. For example, for s = 3.0 mm (Figure 2.9) the values of CHF for θ = 90°, 0°, and 180° are 19.5, 16.0, and 7.5 W/cm^2, respectively. Because the vapor accumulation prevents the liquid from replenishing and rewetting the heater surface, the superheat for CHF also decreases with q for a given s in the same order as CHF, as can been seen from Figures 2.9 - 2.12.

14
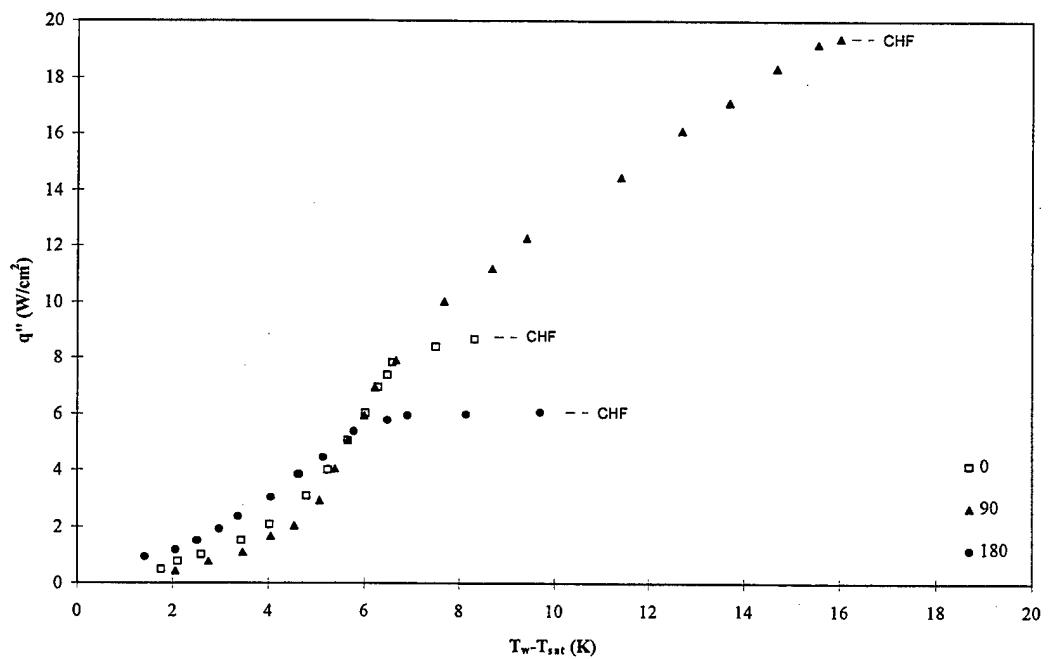
Figure 2.10   Heat transfer characteristics for s=2.5 mm
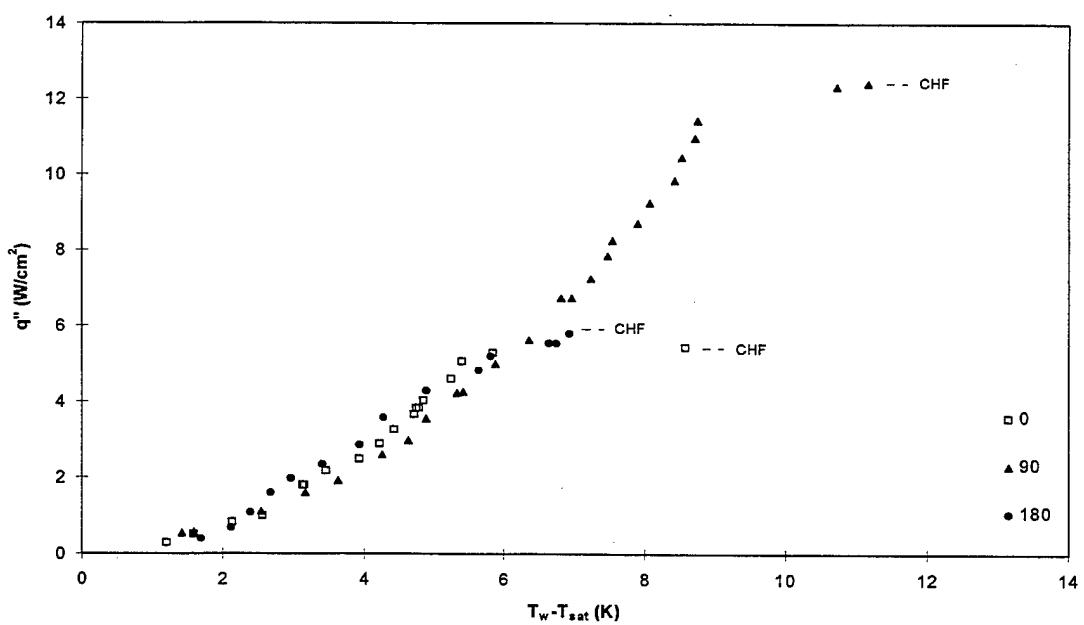
Figure 2.11   Heat transfer characteristics for s=1.5 mm
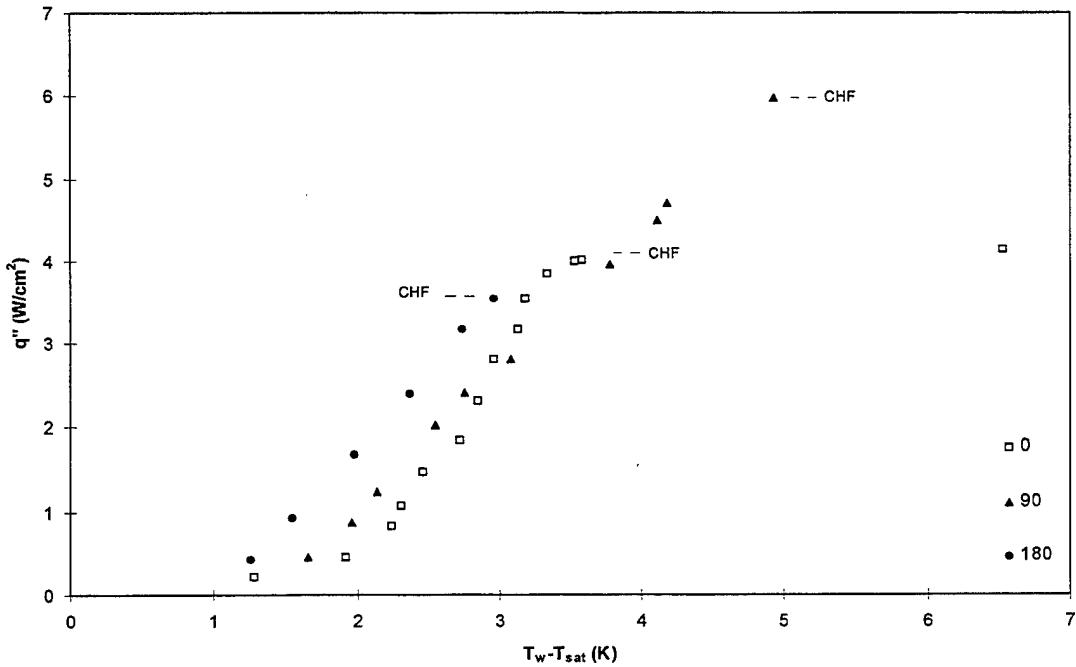
Figure 2.12   Heat transfer characteristics for s=0.75 mm

For a given q, the CHF decreases with decreasing s. The values of CHF with $\theta = 0°$ are 16.0, 8.5, 4.7, and 4.0 W/cm^2 for s = 3.0, 2.5, 1.5, and 0.75 mm, respectively (see Figures 2.9 - 2.12). For $\theta = 180°$, the CHFs are 7.5, 6.0, 5.5, and 3.5 W/cm^2 for the four spacings in decreasing order. The vapor bubble appears to be more readily filling up the gap and pressing against the heater surface as the spacing is decreased. It is noted that values of CHF and ΔT for CHF at $\theta = 180°$ are smaller than those at $\theta = 0°$. This is similar to the open pool boiling, i.e., in addition to the effects of confinement buoyancy force acts to press vapor bubbles against the heater surface.

It can also be noted that for low superheat of Figures 2.10 - 2.12, the heat transfer coefficient h increases as q is increased from $\theta = 0°$ to 180°. One explanation is that the pressing and sweeping motion of vapor bubbles over the heater surface before completely escaping to the ambient help to reduce the liquid layer thickness and enhance the temperature gradient in the liquid layer and thus the heat flux. For example, the differences in value of q'' at $\Delta T \approx 2K$ for s = 0.75 mm increases from approximately 0.4 W/cm^2 at $\theta = 0°$ to 1.6 W/cm^2 at $\theta = 180°$. However, this explanation deserves further investigation because it may not be likewise applicable to open boiling (e.g., for $\Delta T \approx 6 - 8K$ in Figure 2.5 the heat transfer coefficients for $\theta = 0°$ is greater than those of

16

$\theta = 180°$ for the same superheat). The pressing effect is expected to be increasingly significant for $\theta = 0°$ when s is decreased. Take for example $\Delta T = 3K$ in Figures 2.9 - 2.12. The heat flux increases from approximately 1.0 to 3.0 W/cm^2 as s is decreased from 3.0 mm to 0.75 mm. This implies that a sufficiently small spacing can cause similar effects in reducing liquid layer thickness and enhancing heat transfer coefficient as found in downward-facing situations. Similar effects on heat transfer coefficients can also be observed for $\theta = 90°$ and $180°$ in Figures 2.9 - 2.12.

In Figure 2.13, the effect of confined spacing on CHF is depicted for θ other than those of Figures 2.9 - 2.12. In the figure the data for open pool boiling are represented by s = 5.0 mm. It is seen that the values of CHF for each θ ($\pm 30°$, $\pm 60°$, and $90°$) are essentially the same for s $\geq$ 2.5 mm, except those of $\theta = 30°$. There appears to be a value of s above which the effects of confinement are insignificant. For the heater orientations of Figure 2.13 this value is 2.5 mm.

However, it should be noted that such a value of s for $\theta = 0°$ and $180°$ may be larger than 3.0 mm because the values of CHF for s = 3.0 and 2.5 mm are quite different. The values are 16.0 and 8.5 W/cm^2, respectively, for $\theta = 0°$ as can be seen by comparing results of Figures 2.9 and 2.10; for $\theta = 180°$, they are 7.5 and 6.0 W/cm^2, respectively. Furthermore, the values of CHF with $\theta = 0°$ are 26.7 and 19.5 W/cm^2 for open pool boiling (Figure 2.6) and s = 3.0 mm (Figure 2.9), respectively. It appears that the effective spacing for open pool boiling for $\theta = 0°$ would be much larger than 3.0 mm. The CHF are 9.4 and 7.6 W/cm^2 for open pool boiling (Figure 2.6) and s = 3.0 mm (Figure 2.9), respectively. The effective spacing may therefore be a function of the heater orientation. It is worth noting that for the five θ's of Figure 2.13, there is a mechanism for the vapor bubbles to escape, while the mechanism does not exist for $\theta = 0°$ and $180°$. It is also noted that the difference between CHFs with s = ∞ and 3.0 mm for $\theta = 0°$ is larger than that for $\theta = 180°$. This may be attributed to the fact that by decreasing s from ∞ to 3.0 mm, the heater with $\theta = 0°$ becomes pressed by the bubbles accumulating on the confining plate. For $\theta = 180°$, the bubbles press against the heater even for s = ∞. As shown in Figure 2.13, CHF for $\theta = 30°$ continues to increase as s is increased from 3.0 mm to ∞, much similar to $\theta = 0°$ and unlike $\theta = 90°$, -30°, or $\pm 60°$.
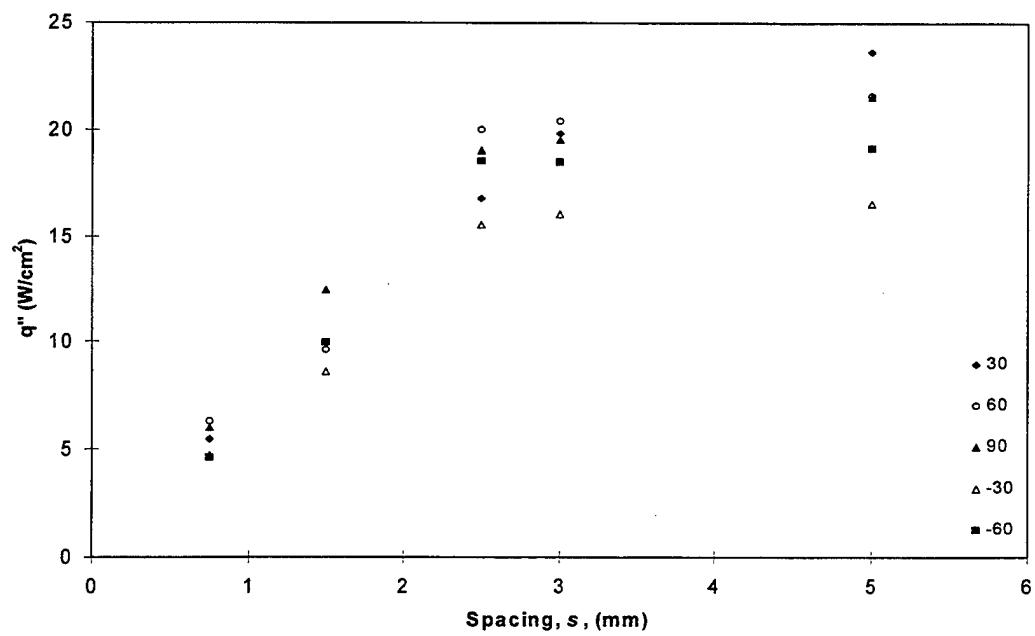
Figure 2.13   Variation of CHF
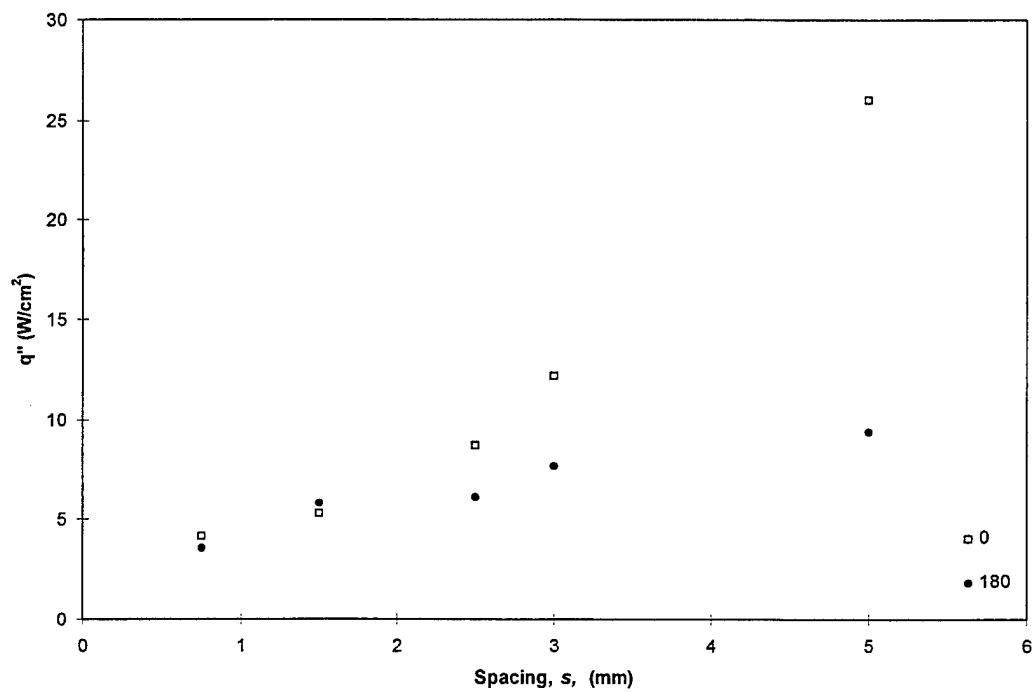
Figure 2.14   CHF for 0° and 180°

18

As s is decreased for each of the five values of θ, CHF decreases in each case. The reduction in CHF is as high as a factor of 4 from s = 3.0 mm to s = 0.75 mm. As can be seen from Figure 2.13, for θ = 30° and -60°, the reductions in CHF are from 18.6 to 4.6 W/cm^2 and from 19.6 to 4.6 W/cm^2, respectively. Similar reductions can also be seen in Figure 2.14, where the reduction factors are approximately three and two for θ = 0° and180°, respectively. The reduction is more significant for the upward-facing heater. This is again believed to result from the fact that the orientation changes from one nearly free of bubbles pressing against the heater surface (i.e., similar to open pool boiling) to another having pressing bubbles. It can be concluded that as the confinement spacing decreases below critical value (≈ 2.5 - 3.0 mm in this study), it affects the order of CHF as a function of θ, as compared to open pool boiling. The effects are qualitative as well as quantitative. A vertically oriented heater leads to the largest CHF for a given spacing. This is, as noted earlier, because it is the only orientation that allows efficient bubble escape from the heater surface.
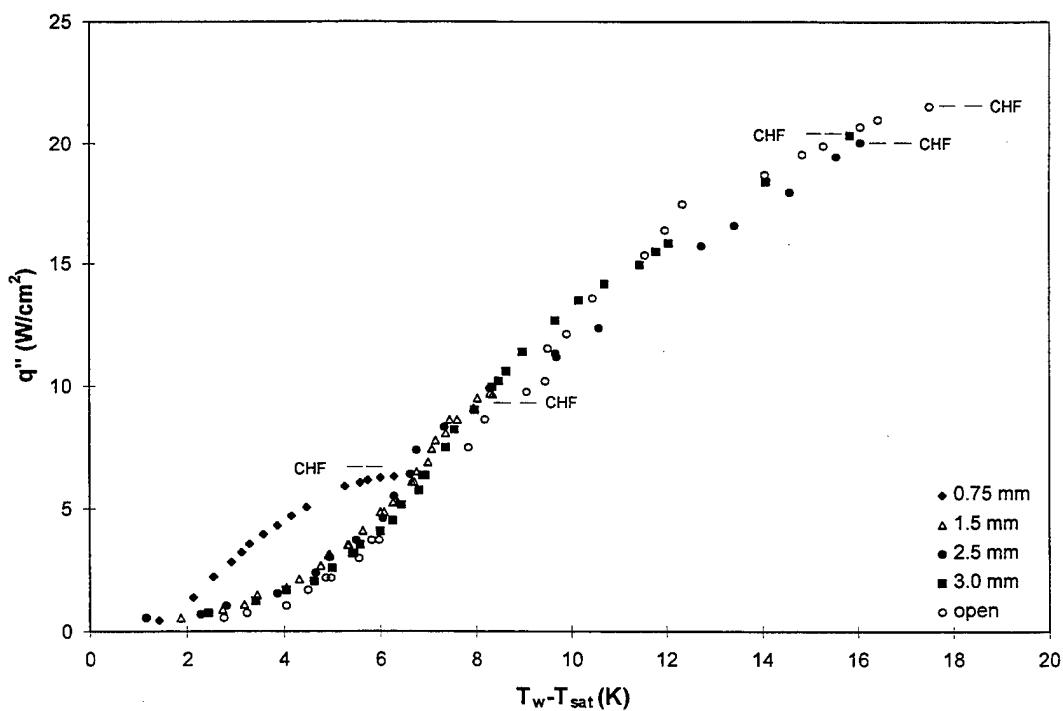
Figure 2.15   Heat transfer characteristics for θ=30°
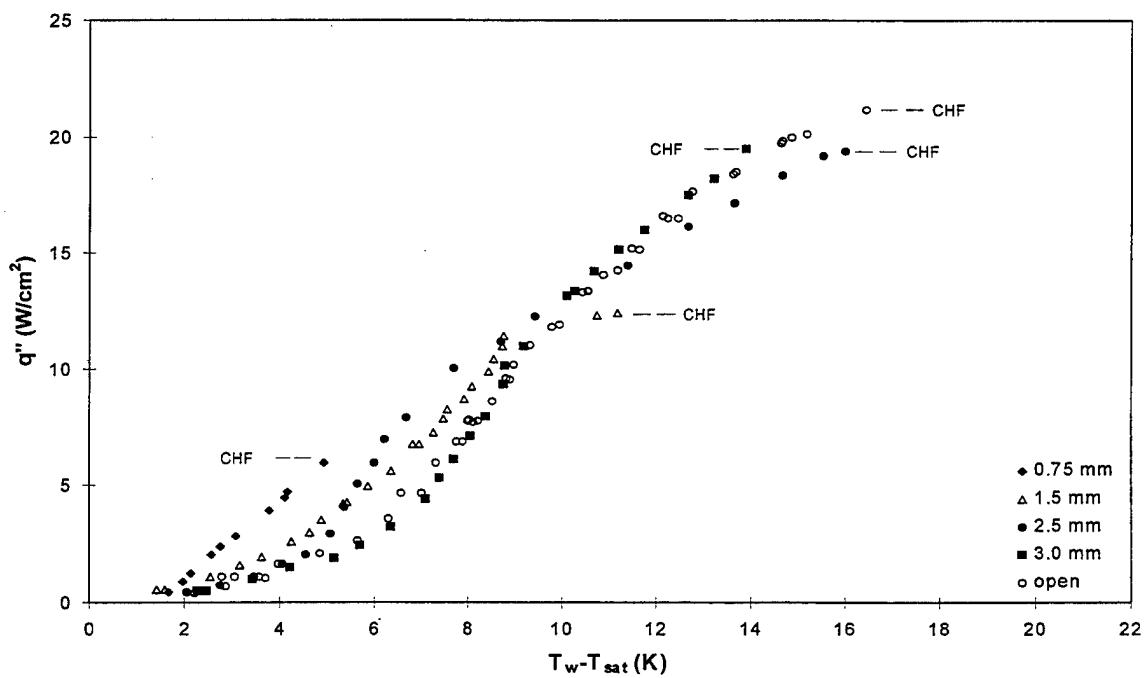
Figure 2.16   Heat transfer characteristics for θ=90°
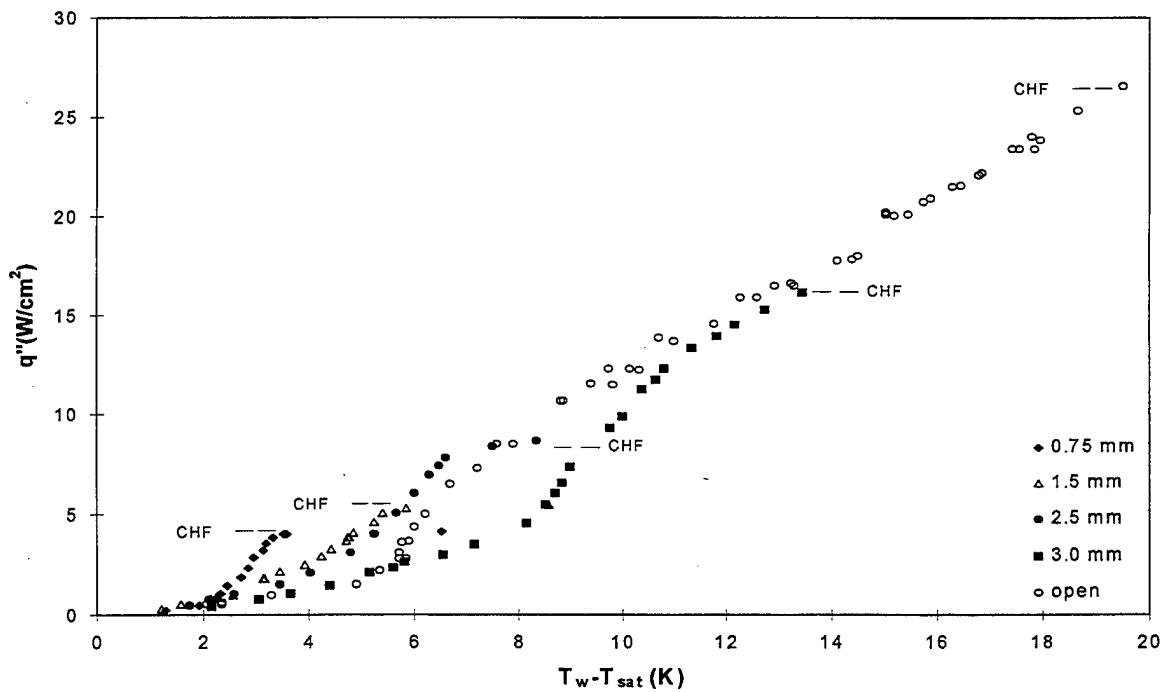
Figure 2.17   Heat transfer characteristics for θ=0°

20
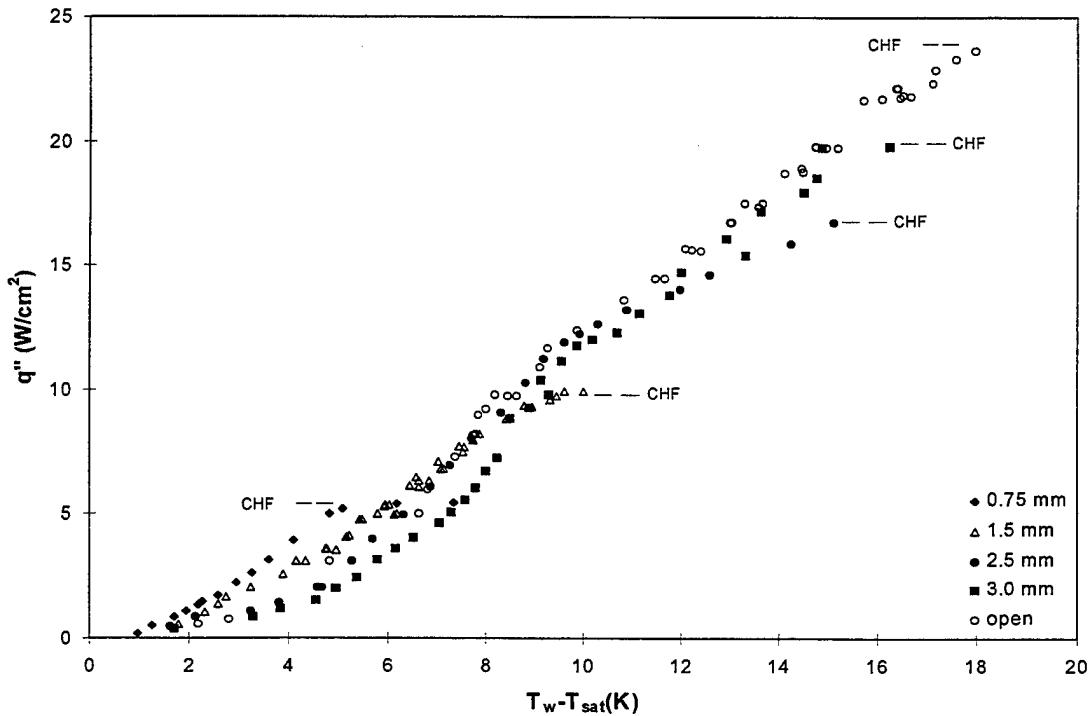
Figure 2.18   Heat transfer characteristics for θ=30°

Further data, for given θ = 0°, 30°, 60°, and 90°, with five different spacings are presented in Figures 2.15 - 2.18.   Observations similar to the ones discussed above can be made: (1) CHF decreases and occurs at lower superheat with decreasing confinement spacing; (2) for s ≥ 2.5 mm the value of CHF does not change significantly; and (3) for a given low superheat the heat flux and heat transfer coefficient increase with decreasing spacing.

2.4.3 Effects of Operation with Heater Array

The heater module in this part of the study had no confining plate in front of it. It therefore constitutes open boiling with a column of heaters with same heat flux. Three orientations (θ = 0°, 90°, and 180°) were studied and the results are presented in Figures 2.19 - 2.21.

Results of Figure 2.19 show that the heat transfer coefficient and CHF (25.6 W/cm^2) of heater No. 9 (Figure 2.2) are similar either operated alone or with other heaters. When facing

21

horizontally upward, the heaters do not appear to feel the existence of others. When facing downward with $\theta = 180°$, the CHF is lower when operated with other heaters (9.5 W/cm^2 vs. 11.75 W/cm^2; see Figure 2.20). Therefore, the heaters "see" each other at $\theta = 180°$. A feasible explanation is that there are more vapor bubbles that have to escape through the same exit area as that for a single heater operated alone. This leads to a slower rate of bubble removal and a lower liquid replenishing rate at surface and, therefore, a lower CHF.

At $\theta = 90°$, the upper heater definitely feels the existence of the lower heater through the bubble rising from the lower heaters and the induced convective flow. The values of the CHF of the upper heater are 24 W/cm^2 and 21.5 W/cm^2 while operated alone and with others, respectively (Figure 2.21). A question arises as to how the induced convective flow would reduce the CHF of the upper heater when it is known that convective boiling should yield higher values of CHF. Similar phenomena have been experimentally observed [6] but the mechanism is not clearly known. Further study is needed for the answer to such a question.
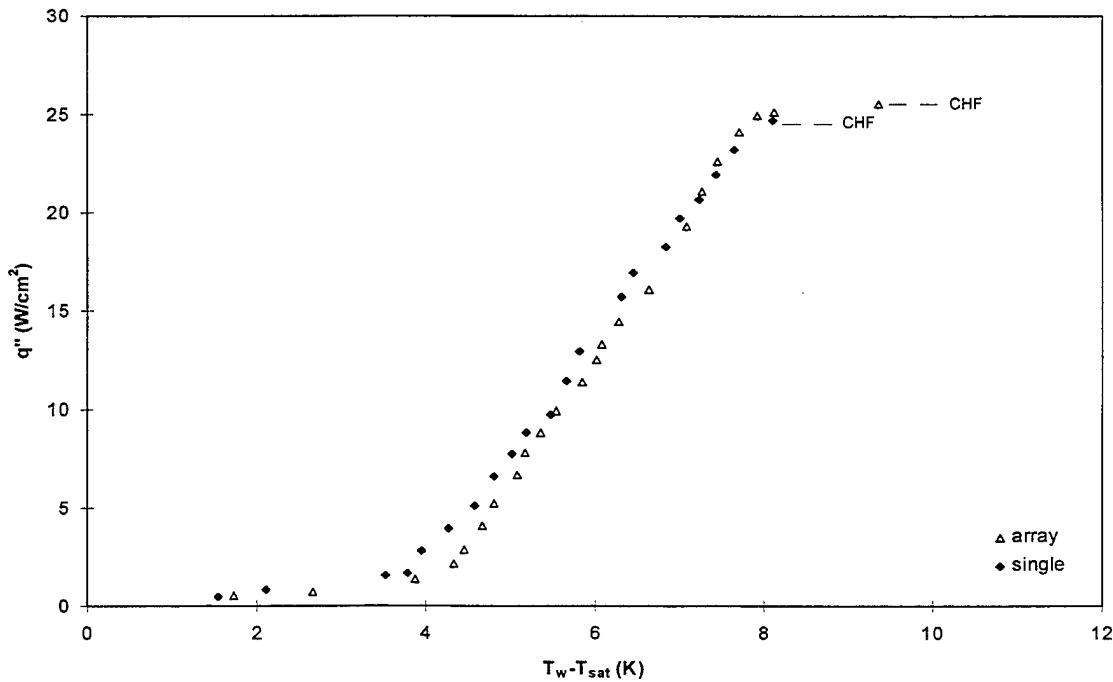
Figure 2.19   Effect of heater array at $\theta = 0°$
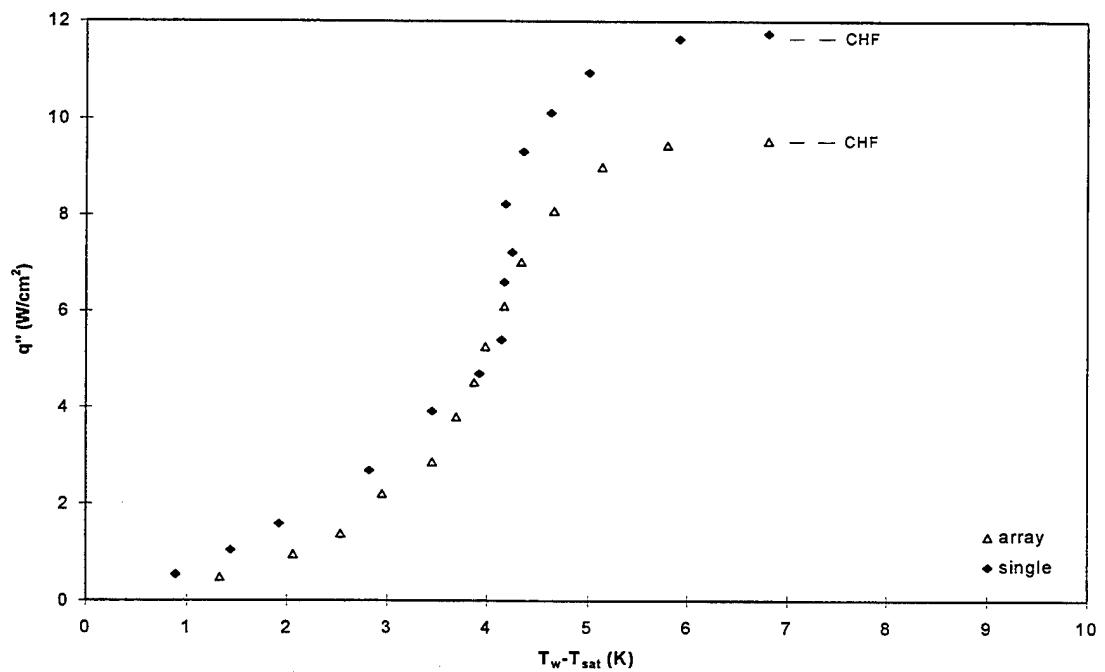
Figure 2.20   Effect of heater array at θ=180°
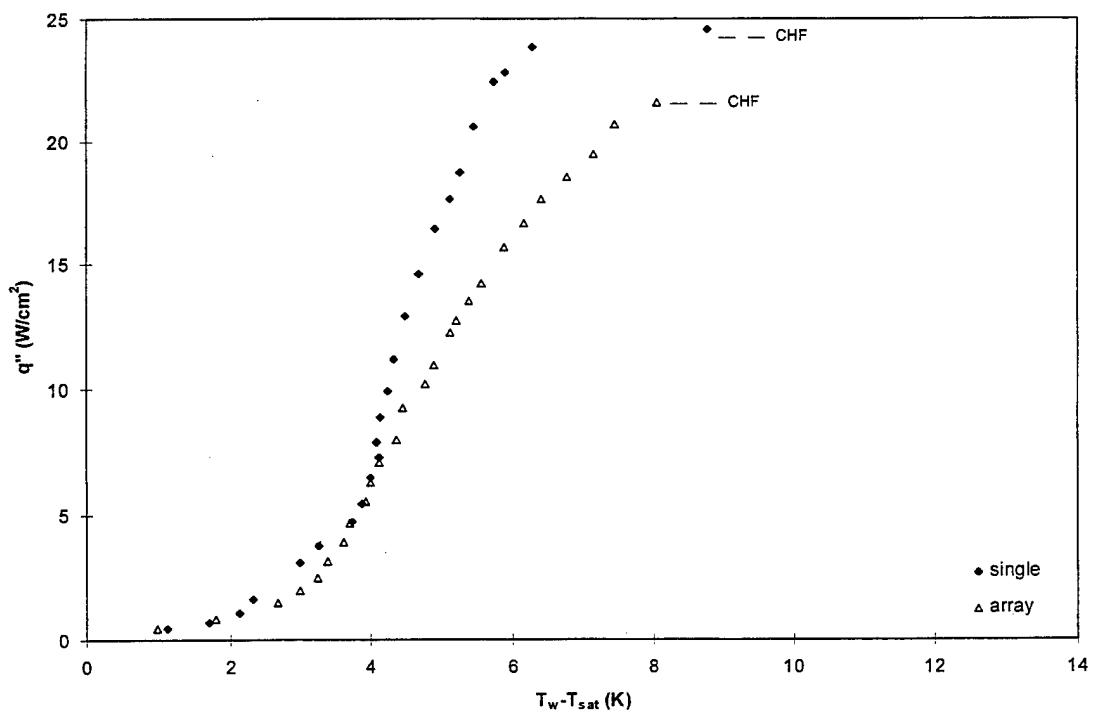
Figure 2.21   Effect of heater array at $\theta = 90^\circ$

3. FORCED CONVECTIVE BOILING IN LIQUID NITROGEN FROM DISCRETE HEAT SOURCES

3.1 Introduction

This task mainly focuses on the research performed on forced convective boiling heat transfer from a discrete source in a rectangular flow channel using liquid nitrogen. This topic is relevant to the direct immersion cooling of electronics by a dielectric fluid. The experimental study dedicated to the effects of flow rate, flow channel geometry, and heater geometry on convective boiling and the visualization of the phase change phenomena. Aside from the two-phase heat transfer study, experiments with gas nitrogen were also conducted.

Direct immersion offers the effectiveness in heat transfer result and simplicity in design implementation. Cryogenic cooling using direct immersion technique is becoming the hot topic in the electronic industry not only because of all the advantages in direct immersion, but also because the cryogenic operation temperature enables the electronic chips to function faster and more accurately. Liquid nitrogen is the favorable working fluid in the applications since it is an economic, nontoxic, environment-safe and dielectric cryogen.

Boiling heat transfer is considered to be very effective as compared to other conventional means of cooling techniques. Such effectiveness is characterized by the fact that boiling heat transfer can attain relative large amount of thermal energy for a small temperature difference. In other words, boiling heat transfer can achieve a high heat transfer coefficient.

The most used direct immersion cooling methods are pool boiling and flow boiling. The boiling heat transfer in this study is characterized as flow boiling. Pool boiling is the most thoroughly studied topic. As opposed to pool boiling, flow boiling occurs with a flowing fluid, and can be further divided into two categories: boiling inside continuously heated tubes or channels and boiling from small discrete heat sources in a channel. The former case, which is pertinent to nuclear reactor cooling, is studied more intensively. While liquid flows along the

25

tube or channel, it absorbs the heat and evaporates continuously. Therefore, the net vapor generation becomes an important factor in the heat transfer as pipe length increases. This encompasses the well-studied area of two-phase flow, which is still not completely understood and nonetheless difficult to model. For the boiling from discrete surfaces of a size of the order of electronic chips, the volume of vapor generated from the heater is generally small relative to the bulk liquid flow over the surface, in other words, the void fraction is small. In such case, the effects of net vapor generation are much less important. This is a relative new area of study however, because it is triggered by the recent dramatic development of electronic industry. The need to remove large amounts of heat from a small surface (high heat flux) has never been so urgent.

Another boiling heat transfer topic of interest is the characteristics of various boiling regimes. As a fluid is heated, boiling starts from discrete sites. Bubbles begin to emanate from these sites. As the heat transferred to the fluid increases, the number of sites increases and gradually the discrete bubbles turn into vapor columns or jets. This regime is termed "nucleate boiling." Nucleate boiling regime is the most desired cooling condition since it is the most effective. As the heat supplied to the surface is increased, a point is reached where the nucleate boiling mechanism breaks down and a transition to a much less effective film boiling mechanism occurs. This transition is also marked by a large and sudden excursion in surface temperature while the heat flux stays unchanged. Such heat flux is also called "critical heat flux" (CHF) in the literature. Film boiling is identified by a thin layer of vapor film that separates the heated surface from the liquid. Under this circumstance, a large temperature difference is required to transport the same amount of heat through this vapor layer. Consequently, film boiling is not desirable. From the above discussion, obviously it is very import to determine the point at which the CHF occurs in the application of boiling heat transfer. This research studies the variation of the CHF with the flow condition as well as the geometry effects.

3.2 Background

A vast amount of experimental work has been performed trying to develop a means of cooling the high-speed, large-scale circuits envisioned to be in service in the future. An excellent

review of this work is by Incropera [8]. Other assessments of electronic cooling technologies have been given by Bar-Cohen [9], Chu [10], and Nakayama [11]. As electronics cooling requirements have become more demanding, complex air cooling designs are gradually yielding to equally complex yet much more effective liquid cooled designs. Among the proposed liquid cooled designs, those designs incorporating phase-change are by far the most predominant. Two-phase (or boiling) heat transfer has two distinct advantages over single-phase heat transfer. First, it can achieve higher heat fluxes for a given operating temperature. Second, phase-change heat transfer can obtain a high heat transfer coefficient. Since phase-change generally occurs at a fixed temperature (boiling point), heat flux can vary substantially with only small changees in temperature. The heat transfer process occurs at such a fixed point. This makes it easier to implement temperature control of electronic devices, which is one of the important reasons why such a boiling heat transfer design is so noticeable. Temperature control is extremely important because electronic failure rates approximately double for every 10° C rise in operating temperature [12]. It is well understood that single-phase heat transfer methods (such as microchannel cooling) require a much larger temperature difference for similar change in heat flux and are not as desirable from a thermal stress and reliability point of view.

Direct immersion proved itself to be a highly effective cooling technique. In order to implement direct immersion, dielectric liquids must be chosen. The common coolants used in the direct immersion applications are: R-113, fluorocarbon (FCs), liquid nitrogen, and liquid argon. Extensive research has been conducted of pool boiling from small heat sources using R-113 by Baker [13]. A CHF of 20 W/cm^2 with zero subcooling was achieved. Similar experiments with chips and substrate assembly cooled in FC-86 pool were conducted by Hwang and Moran [14]. They also reported the effect of restricting boiling in a narrow space situation. Other researchers like Megerlin and Vingerhoet [15] determined that CHF from FC-78 was around 15 W/cm^2. Lots of research concerning forced convective flow boiling with the direct immersion methods have been conducted. As early as the 1970's, Baker [16] used Freon 113 to obtain a CHF as high as 200 W/cm^2. Baker focused his study in a single small heated surfaces to simulate individual IC chips and other types of compact electronic devices. Later on, McGillis and Carey [17] began to concentrate on an array of heat dissipating elements, which represents the practical electronic devices consisting of many electronic packagings. Several visualization

experiments were also attempted. Gunther [18] reported a vapor accumulation on downstream heater locations as CHF approached. Galloway and Mudawar [19] were able to obtain clear pictures about the flow boiling with FC-87, a 3M dielectric fluid. Many researchers began to realize the increasing importance of electronic cooling. Much work has been done on discrete small heated elements. In flow boiling, the simplest and most common setup of IC (Integrated Circuit) chips is in-line array. Gersey and Mudawar [20] did a lot of valuable experimental studies with in-line heater under flow boiling conditions. They also pointed out the effects of heater orientation on CHF values. The most recent work was carried out by Leland [21]. A number of factors that affect flow boiling conditions have been probed. This includes the effects of flow channel heights, channel curvature and the relative position of heaters and the flow channel. Leland used coolant FC-72 in his experiments.

Cryogenic cooling becomes a hot topic in the electronic cooling field because recent studies point out that IC chips operating at cryogenic temperatures can improve circuit performance and decrease their size. The easiest cryogenic cooling to apply is the liquid nitrogen pool boiling. Liquid nitrogen is an economic, nontoxic and dielectric fluid, whose saturation temperature under one atmosphere pressure is 77 K. Numerous benefits of operating electronics at low temperatures can be realized with liquid nitrogen cooling. Chui et al. [3] conducted pool boiling experiments on an array of rectangular heaters (21.7 mm x 17.4 mm, each heater). They were able to achieve CHF to 16 w/cm^2 in the vertical orientation. The experiment of pool boiling with a limited space in front of the array (constraint spacing) determined that the heat transfer coefficient and the CHF value were affected greatly when the space limit was below 1.6 mm. Later in this annual report, it can be seen that research on the liquid nitrogen pool boiling was continued with an array of nine heaters (20.3 mm x 10.1 mm, each heater). Experiments were conducted in order to investigate the topic further on orientation and limited spacing effect. It was found that with such heater array, CHF was around 26 W/cm^2 with the heaters facing upward. The space constraint deteriorated the heat transfer condition. While the spacing was under 2.5 mm, the effect on CHF was very significant.

As the number of chip level components and gates increase as result of the development of very large scale integrated (VLSI) and ultra large scale integrated (ULSI) chip technologies, the dissipated heat and consequently the heat flux of IC's have also increased. Such advanced

applications of high-performance electronic components require special cooling techniques to remove high density power dissipation from microelectronic chips. Under such demanding high heat flux requirements, pool boiling can no longer satisfy the needs. Therefore, other types of enhanced heat transfer mechanisms are developed. The most commonly considered technique is force convective boiling. However, the previous work of using liquid nitrogen flow boiling for electronic packaging cooling is almost nonexistent. Early heat transfer research focused on traditional setups such as continuously heated pipe flow, etc. The results obtained from these types of experiment cannot be used in electronic cooling setups, where the heated sources are discrete, small IC chips. There is a demand for experimental and theoretical analysis of electronic cooling using cryogenic fluids at this stage.

Moreover, there has never been an observation of the boiling phenomena of liquid nitrogen. Visualization is becoming more and more important in understanding phase-change processes and establishing a mathematical model. Many visualization experiments were carried out. Leland et al., [21] has done visualization experiments on flow boiling with FC-72. Galloway and Mudawar [19] took pictures of flow boiling from a very narrow flow channel. They also approached the theoretical model based on what they observed from the phase change phenomena. Due to the practical difficulty in carrying on visualization experiments with liquid nitrogen, little work has been done. Chui [3] successfully built a visualization setup for pool boiling. As far as flow boiling with liquid nitrogen, visualization has never been attempted.

3.3 Experiment Setup and Procedure

3.3.1 Experiment requirements and objectives

The experiment setup has been designed to be transparent to allow visualization. The test section must be flexible enough to allow variable flow channel heights. It also needs to be assembled in such a way that it is easy to change heaters of different dimensions and vary the distance between heaters.

The experiment focused on determination of the CHF value, heat transfer coefficient and heater surface temperature while other factors are varied. These factors include: liquid nitrogen flow velocity, heater dimensions, heater geometrical arrangements, multiple heaters and flow channel height.

3.3.2 Experiment Setup Design

3.3.2.1. Material Selections and Tests

The experiment setup must be transparent to allow visualization. During the experiment period, the materials repeatedly experience vast temperature change from room temperature (300 K) to liquid nitrogen temperature (77 K), and back to room temperature, which leads to significant thermal contraction and expansion and therefore, thermal stress. The best transparent material which has a relatively small thermal expansion coefficient and large mechanical strength is quartz glass. However, glass is not machinable. It is very difficult to put threads in the glass chamber and connect the glass chamber to pipeline fittings, valves and measurement equipment. It is found that Plexiglas might be the only useable material. After carefully examining the physical and chemical properties of a number of Plexiglas materials, we narrowed our selections to two similar materials: Acrylic and Polycarbonate. Acrylic provides excellent light transmission. It is significantly more shatter-resistant than glass. Acrylic also has superior strength and durability, good machinability, and dimensional stability. Polycarbonate has great impact strength, excellent machinability and better temperature resistance. However, it is not as strong as Acrylic. Both materials have their own chemical adhesives, which can glue them together. It was demonstrated that the glue bond area has higher strength then the rest, which is an important advantage because those glue areas are usually highly stressful areas.

Both materials have been tested with liquid nitrogen. The test consists of two phases. Phase 1 was the thermal shock test phase. Two (2) half boxes were made using Acrylic and

Polycarbonate; they were set inside a cryogenic dewar. Liquid nitrogen was then directly flown towards the boxes, creating an environment where its temperature dropped drastically from 300 K to 77 K within about 2 minutes. The boxes simulated rapid submersion in liquid nitrogen. It was proven that both materials could withstand the thermal shock. The boxes did not crack and the glue was still bonding the pieces together. The Phase 2 of the test was the thermal fatigue experiment. The two Acrylic and Polycarbonate boxes were cooled down and then warmed up repeatedly to simulate the real experimental conditions. They both passed the test as well. Acrylic was finally chosen to build the cooling and vacuum chamber (details about the setup will be described later in this chapter), which could stand the system pressure of 25 psig. Polycarbonate, with its better temperature flexibility was chosen to build the test section.

3.3.2.2. Experiment Setup I

The first experiment setup was built based on the schematic view (Figure 3.1).
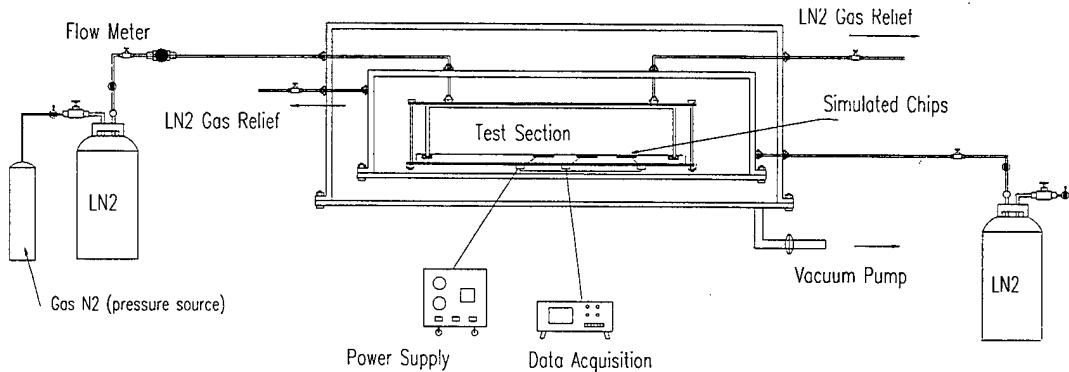
Figure 3.1   Schematic View of Apparatus

The experiment apparatus had four primary components; the test section, the cooling chamber, the vacuum chamber and the data acquisition, and measurement and power supply section. There were a total of two flow loops. The test section was made of Polycarbonate. The cooling chamber and the vacuum chamber were made of Acrylic. The wall thickness was

approximately 1/4 inch. The tubes were copper tubing 1/4 inch in diameter. Tube fittings were purchased from the Swagelok company, which were made of stainless steel.

The test section consists of the flow channel and the heater assembly modules. The width of the flow channel was three inches, the height was 1/4 inch, and total length was 16 inches. There were three heater modules simulating three electronic chips embedded in the base piece of the test section. The dimension for the heater assembly module was 0.9 x 0.7 inch, which left about 1 inch space from the edge of the heater module to the boundary of the flow channel. The first module was placed about nine inches away from the entrance . The distance between each heater module was equal to one inch. Therefore, after the last heater module, there was another 2.3 inches remaining to the exit. This was designed to avoid turbulence from the exit which could affect the last heater.

The cross-section view of the assembly module is shown on Figure 3.2.

Copper Block

Indium Sheet

Heater Ceramic Base

Soldering Strip
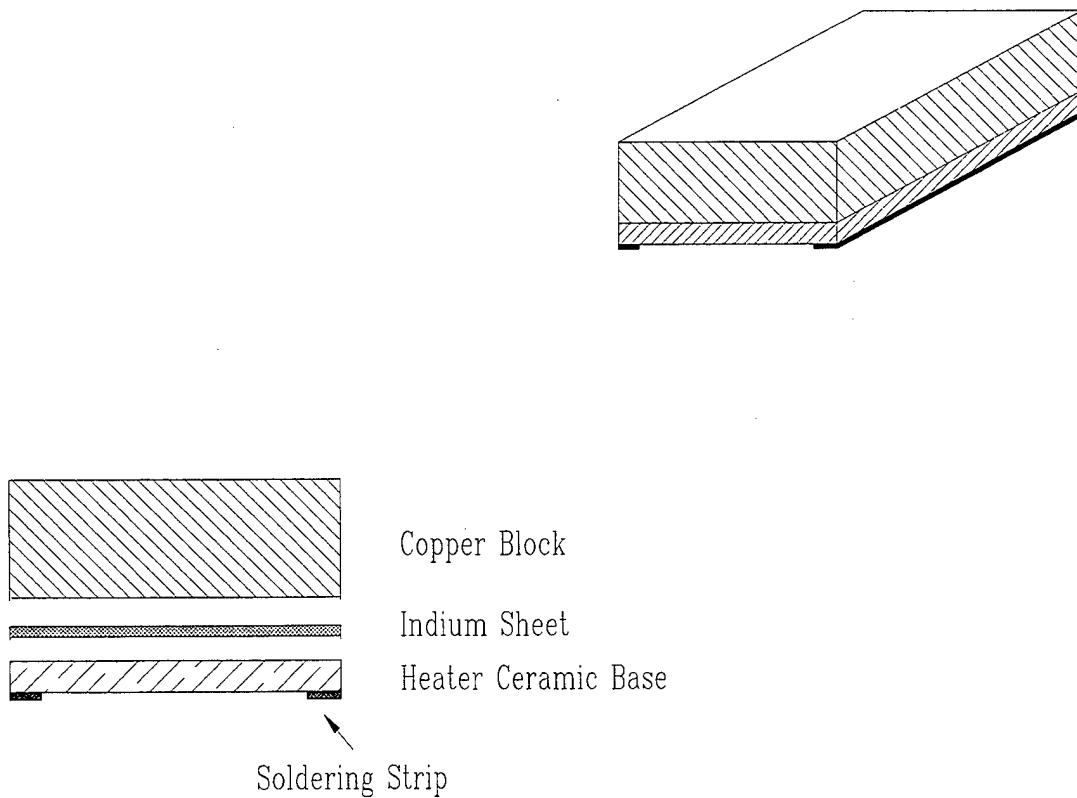
Figure 3. 2   Heater Assembly Module

The heater consists of two parts. The top part was an oxygen-free electronic copper block, 99.99% pure. The dimension of the block was 0.9 x 0.7 inch, with 0.2 inch of thickness. A small hole with a diameter approximately 0.008 inch was drilled from the side of the copper block to the center. An E-type thermocouple was placed in this hole to measure the surface temperature of the heater. The reason for choosing E-type thermocouples is because they are more sensitive and thus more accurate for measuring cryogenic temperatures. E-type thermocouples also have a relatively low thermal conductivity, good resistance to corrosion in moist atmospheres, and reasonably good homogeneity. For these reasons and their high Seebeck coefficient, E-type thermocouples have been recommended as the most useful for low-temperature measurements. The thermocouples in this experiment are made from E-type wires of diameter not exceeding 0.003 inch. The tip of the thermocouples is no larger than 0.008 in diameter (two individual wires was soldered together). This type of small thermocouple is very sensitive to temperature changes and has a minute time lag.

The bottom part of the assembly module was a fine-film heater. It has a high thermal conductivity ceramic base with resistor film deposited on one surface and soldering film on the other surface. Along the two sides of the resistor film, there were two deposition strips for soldering the power cables. The resistance of the heater used in this experiment setup is 12.0 Ω. All three heaters' resistance were within 0.1 Ω compared with each other.

Alongside the base piece, an O-ring groove was cut to seal the base with the top chamber. The groove was 1/8 inch in width and 0.07 inch in depth. It was filled with clear silicon rubber sealant.

The base piece of the test section which contained the three heater modules can be exchanged with other base pieces easily. This makes it easier for the researcher to vary factors such as the heater dimension and the distance between heaters. It also lets the researcher adjust the flow channel height relatively easy. Flow channel height is another important factor which affects the CHF value and heat transfer phenomena.

The cooling chamber was designed such that the test section would be totally immersed under liquid nitrogen. This chamber served as the best insulation one can obtain in cryogenic experiments. Liquid nitrogen has a boiling point of 77.8 K under one atmosphere pressure, which means there exists almost 250 K temperature difference with the environment. The heat leakage into the system under such a huge drive of temperature difference is very significant. Another reason to design the cooling chamber is because the experiment setup is totally transparent. The radiation from the surroundings into the test section cannot be neglected. During the experiment, the cooling chamber was supplied and filled with liquid nitrogen. Therefore, the test section which was submerged under the liquid nitrogen gained a perfect insulation from its surroundings. With this design, the test section was completely separated from any heat source except the heaters inside.

Outside the cooling chamber is the vacuum chamber. When liquid nitrogen was filled inside the test section and the cooling chamber, the huge temperature difference of the room temperature and liquid nitrogen temperature makes the liquid nitrogen inside boil violently. The bubbles generated on the wall of the cooling chamber obstructed visualization to the test section. In the meantime, since the wall of the cooling chamber is extremely cold, the water vapor on the outside wall of the cooling chamber condensed and formed a thick ice insulation, which also eliminated the possibility of clear visualization. For these two reasons, the vacuum chamber was set up outside the cooling chamber.

All thermocouples were calibrated according to the manufacture's procedure and standard before installing them. A highly accurate voltage meter was used to carry out the calibration. Keithley 2000 is a 6-and-a-half-digit high performance digital multimeter, which has a resolution of 0.1 μv. Considering the voltage signal generated from type E thermocouples, it can be calculated that the temperature measurement can be accurate to within 0.00348 °C. The data acquisition program used the polynomial conversion equation (from voltage signals to temperature readings) provided by the manufacturer of the digital multimeter. The overall accuracy of the temperature measurement of this multimeter can be as good as $\pm$ 0.3 °C while remaining within the temperature range of 37 K to 300 K. The resolution for DC current measurement is 10 nA. Resistance measurement can be as small as 100 $\mu\Omega$.

3.3.2.3. Modifications--Experiment Setup II

Preliminary tests showed that some modifications were needed. The system schematic is show as Figure 3.3.
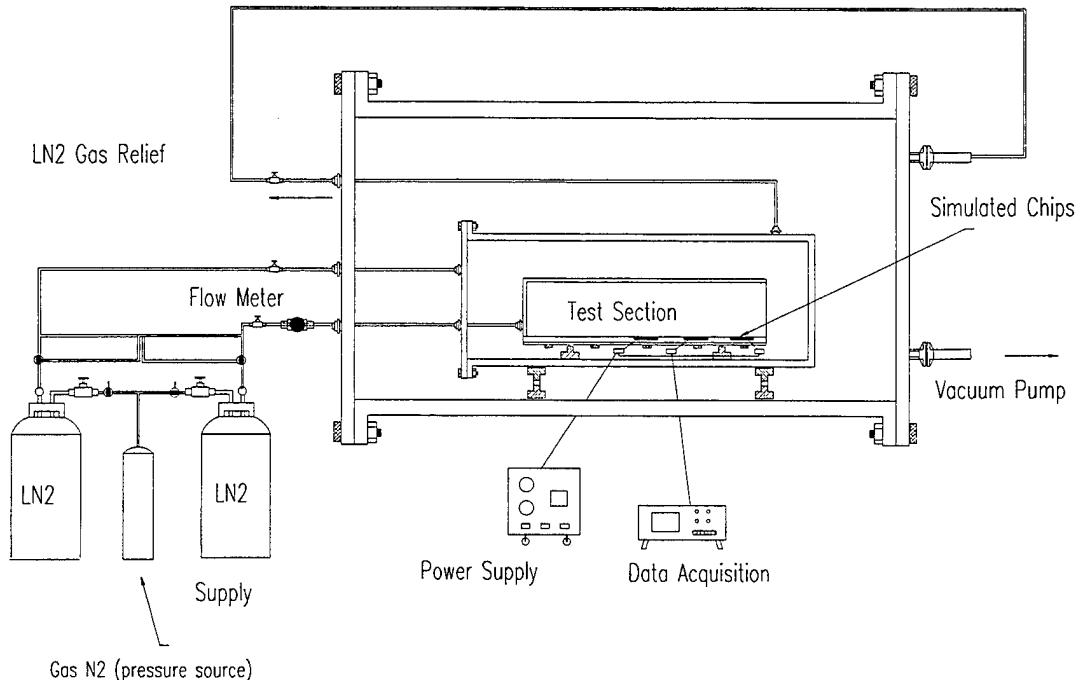
Figure 3. 3   System Schematic

The two flow loops were combined into one simple loop. The test section had an opening at the far side. Liquid nitrogen was supplied from a dewar and flew into the test section from the other side through the pipe and pipe fittings. It then came directly out of the test section and flowed into the cooling chamber. After it filled the cooling chamber, liquid nitrogen would flow back to the second liquid nitrogen dewar. One dewar served as the supply source and the other was an exhaust tank. The test section now had an big opening. It was modified to a box with only five surfaces. Obviously, the pressure drop inside the test section was almost zero. In other words, the pressure inside the test section should be equal to the pressure in the cooling chamber (There existed no pressure difference across the heater modules). The sealing around the heater

modules was thus, easier and better. The minor leakage around the heater was the most serious one. Liquid nitrogen would damage the ceramic base and cause cracks. More importantly, the liquid would also evaporate from the sides of the heater module, which makes the measurement inaccurate. The only allowed heat dissipation was from the top-heater surface. The other five surfaces of the heater module should be made as adiabatic as possible. The pressure difference made the leakage almost inevitable under the cryogenic temperature, since the dramatic temperature drop caused thermal contractions from different types of material. The flow rate must be adjusted easily and quickly. Secondly, the liquid nitrogen must last from the beginning to the end of the experiment, which was between eight and ten hours. Obviously, in order to achieve these two requirements, a close loop must be built. The exhaust nitrogen mixture should not be discarded. The mixture would be recycled to get rid of the vapor content and reuse the liquid. The supply dewar was always under the constant pressure of 25 psig, maintained by the pressure regulator device and the external gas nitrogen cylinder. The exhaust tank was always open to the atmosphere. Therefore, the pressure across the flow loop was constant, which led to the constant flow rates.

3.3.3 Experiment Procedure

Before installation into the test section, the exposed heater surfaces were cleaned with diluted hydrochloric acid to remove any oxides. Then acetone was used to remove finger oil, solder flux and other residue. The heater modules were installed into the test section. The test section then was installed into the cooling chamber. Cables were connected using clips. The whole enclosure was then put into the vacuum chamber. All sealant was allowed a 48-hour drying period before the system was connected to liquid nitrogen.

A special data acquisition program was written to monitor the cooling down process which lasted for six to eight hours. It was vital that the temperature of the system drop slowly and as uniformly as possible. Temperatures inside and outside the test section, as well as the cooling chamber were monitored constantly by the program. After the cooling chamber was filled with liquid nitrogen, the monitoring program would be stopped. The data acquisition program was then executed. The desired flow rate was set by adjusting the feeding valve. After everything was checked, the selective heater(s) was connected to the power supply which was

then switched on. Power was increased in small increments causing the liquid going from single phase convective flow to nucleate boiling regime to CHF. After each increment, temperature was measured and compared to each other repeatedly to determine whether the system reached steady state. Once and only at steady state, all parameters were recorded to the host computer. Then the power was increased again until an extremely rapid and dramatic heater surface temperature overshoot was observed; this is the indication of CHF. The power supply was shut off as quickly as possible to avoid heater burnout. Then the flow velocity or heater geometry was varied and the experiment went on.

3.4   Results and Discussions

3.4.1   Flow Boiling CHF Model

Flow boiling CHF modeling is closely related to the CHF models of pool boiling. However, after over 40 years of development, neither the pool boiling nor the flow boiling CHF models is complete. Haramura and Katto [22] revised the pool boiling CHF mechanism proposed by Zuber [23]. They postulated that there exists a thin layer of liquid called the macrolayer under the vapor bubble mushrooms. The mushroom is the result of coalesced bubbles. The macrolayer is the liquid thin film trapped beneath the vapor mushroom. CHF occurs when the liquid macrolayer dries out before other surrounding liquid can replenish. This model identifies that pool boiling CHF is the result of excessive vapor patch dry out due to the periodically restricted inflow of liquid caused by large hovering vapor mushrooms.

Now that the mechanism of the pool boiling is presented, Haramura and Katto extended the pool boiling model to flow boiling field. They postulated that CHF occurs when the macrolayer is just depleted at the most downstream edge of the heater.
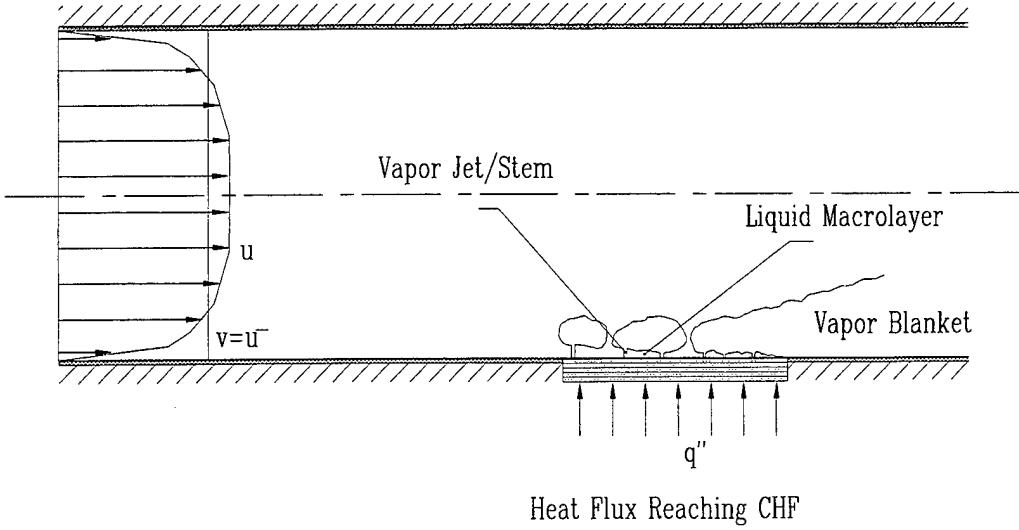
Figure 3. 4   Schematic Representation of Flow Boiling CHF

According to this mechanism, energy balance for the heater gives:

$$q''_{CHF} * L = \rho_f * \delta * U * h_{fg}$$

where L is the heater length along the flow direction, ρ_f is the liquid density, δ is the macrolayer thickness. Numerous versions of the CHF model have been developed by evaluating the macrolayer thickness differently. Katto assumed the macrolayer thickness for flow boiling scenario was the same as pool boiling. His results proved not to be in accordance with the experimental observation of liquid nitrogen.

Mudawar [24] improved the model by introducing the effect of a fully developed turbulence profile. However, the equation derived from his model does not fit the liquid nitrogen experiments either. It is understandable that the models from other researchers do not work perfectly with liquid nitrogen. None of them developed their models from the experimental work with cryogenics fluids. Cryogenic fluids have very unique properties which are significantly different from other fluids such as water, fluorocarbon, etc. It would not be surprised that the

correlation developed from experiment research of these conventional fluids would be extrapolated to liquid nitrogen.

The model developed in this research was based on the macrolayer mass and energy balance. The experiment covered turbulent flow with Reynolds number ranging from 30,000 to 120,000. The liquid nitrogen flow velocities were between 0.6 m/s and 2 m/s. The following equation was derived from the model which was based on turbulent flow velocity distribution profile:

$$q''_{CHF} = 0.0287 \frac{\delta^2}{2} \frac{\rho_l \cdot h_{fg} \cdot (\frac{Ud}{\nu})^{-0.2} \cdot U^2}{L \cdot \nu}$$

where δ is the macrolayer thickness, h_{fg} is the latent heat, L is the heater length, and d is hydraulic diameter of the flow tunnel. The critical heat flux was thus determined by the macrolayer thickness, flow velocity, liquid physical properties, and geometrical effects. Experiments have been conducted after all the modifications on the setup. Many important factors that affect CHF were studied. The CHF value was determined experimentally, thus, the macrolayer thickness δ can be calculated from the above equation. The data collected from the experiments fit the model well. Generally speaking, the macrolayer thickness decreases while the flow velocity increases. The thickness is in the order of several tens of microns.

3.4.2   Effect of flow velocity on CHF

Data was obtained for the CHF value and heat transfer characteristics while the flow velocities were varied. They are shown in Figure 3.5.
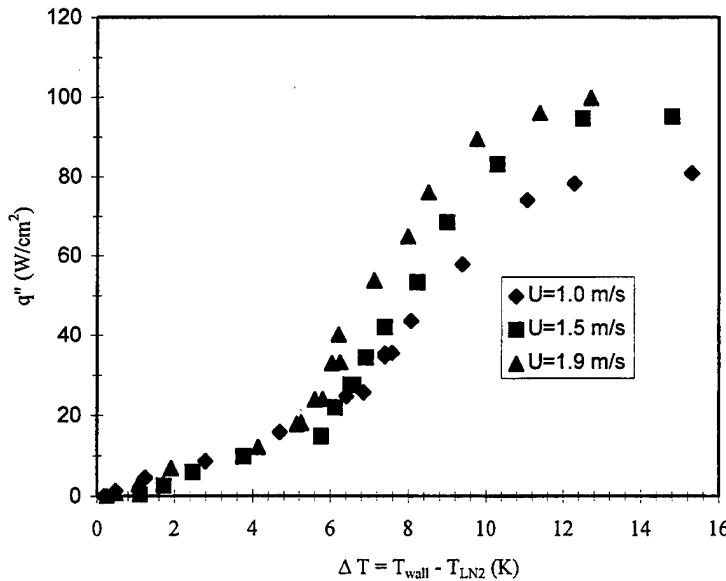
Figure 3. 5   Heat Transfer Character under Different Velocity

The flow channel height was 3.18 mm. The following table summarized the results of flow velocities, Reynolds numbers, CHF values and macrolayer thickness.

Table 3.1   Experiment Results for Various Flow Velocities

	Flow Velocity (m/s)	Reynolds #	CHF (W/cm^2)	Macrolayer Thickness (μm)
1	1.05	33,000	87	61.5
2	1.5	47,000	95	44.0
3	1.9	59,000	103	38.0

According to mechanism of flow boiling, CHF occurs when the liquid macrolayer below the bubble vapor mushrooms dries out. In the flow boiling, the liquid was fed tangential to the surface from the leading edge of the heater. The liquid macrolayer then absorbed the heat engorge from the heater and evaporated. The macrolayer then shrinks in thickness along the direction of flow. Therefore, the liquid supply to the most downstream portion of the heater is the most impeded. Next, dry out initially occurs at the most downstream portion of the heater. The results show that CHF increases with the increase of flow velocity because the improvement

of liquid feeding through the leading edge of the macrolayer by higher velocity. It can also be seen from the results that macrolayer thickness decreases with the increase of flow velocity, which also explains why under high flow velocity, the heat transfer curve shifts to the left. The heat transfer coefficient improves when the flow velocity increases. The same trend was observed in experiments with different flow channel and different heater dimensions.

3.4.3 Effects of Channel Heights

The experiment setup has the capability of changing flow channel heights easily. A total of three different heights were tested.
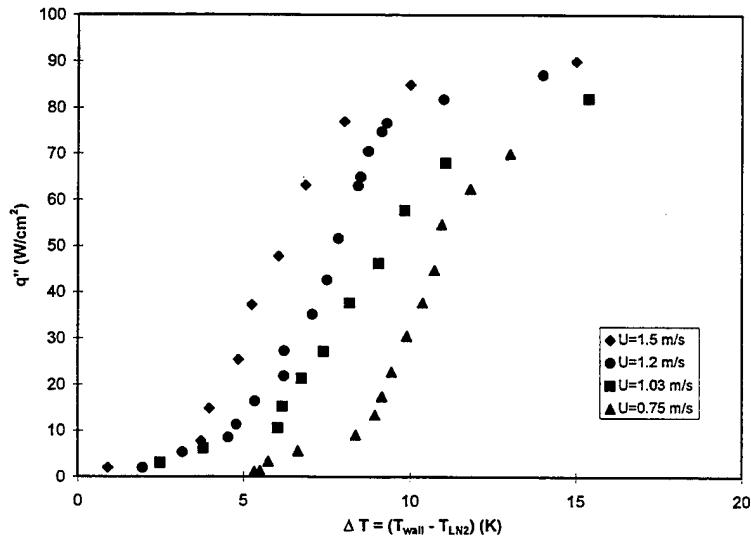
Figure 3. 6   Heat Transfer Characteristics from 1/4-inch Channel Height

Figure 3.6 shows the results from a 6.35 mm (1/4-inch) high flow channel. Compared with the results in Figure 3.5 obtained from the 3.18 mm (1/8-inch) high flow channel, it can be concluded that there were no significant differences between these data sets. Therefore, when the channel height is more than 3.18 mm, the height has no significant effect on the CHF value.

Table 3.2   Experiment Results for 1/4-inch Channel

	Flow Velocity (m/s)	Reynolds #	CHF (W/cm^2)	Macrolayer Thickness (μm)
1	0.75	42,000	70	79.0
2	1.03	59,000	82	72.0
3	1.20	68,000	88	57.4
4	1.50	85,000	92	49.0

The channel height was then further decreased to 1/16-inch. The experiment results were illustrated in Figure 3.7.
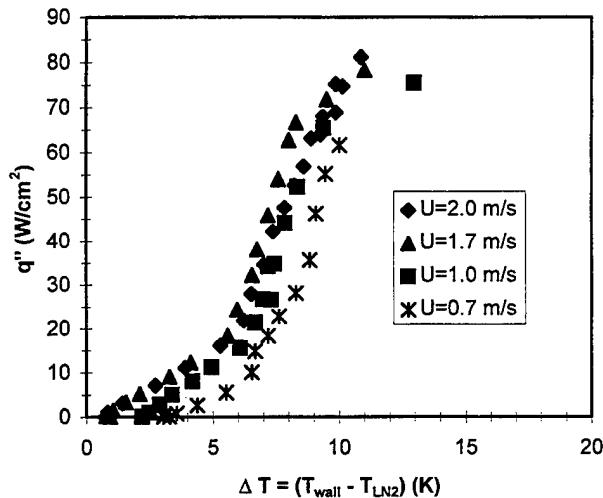
Figure 3. 7   Heat Transfer Characteristics from 1/16-inch Channel Height

The results from the 1.59 mm (1/16-inch) channel were obviously different than those from 6.35 and 3.18 mm channels. The CHF values decreased significantly compared with those obtained from the 3.18 mm channel. Generally speaking, the CHF suffered a 15 - 20% drop. However, the CHF value measured from the 1.59 mm channel were experiencing less drop at lower flow velocities than those measured at high flow velocities (Figure 3.5, 3.6) because of the CHF mechanism.
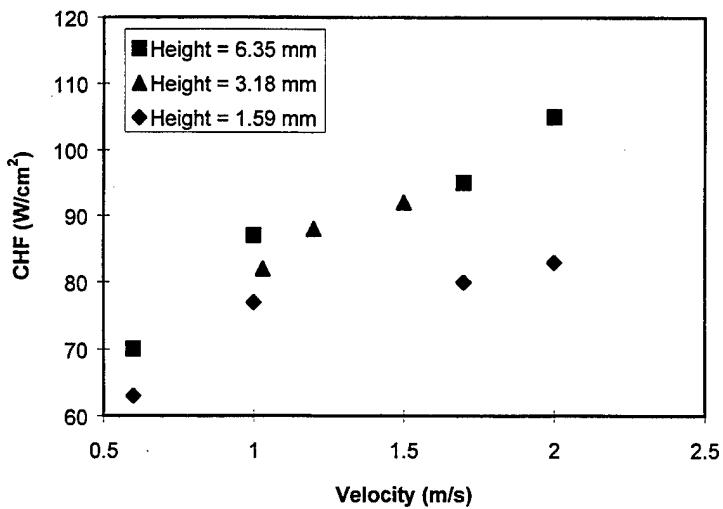
Figure 3.8   CHF Comparison for Different Channel Heights

The occurrence of CHF in boiling depends on two mechanisms: liquid feeding and vapor escaping. During flow boiling, the liquid is fed from the leading edge of the macrolayer. At high flow velocity, the turbulence grows stronger. The vapor layer consisting of bubbles is much thinner and more uniform in thickness over the length of the heater. The bubbles prone to be carried away from the surface of the heater with the flow. The heater is then get replenished by the liquid from the above. Therefore, higher flow velocity delays the occurrence of CHF, leads to high CHF value. At low flow velocity, the first mechanism is dominate. When the channel height drops to 1.59 mm, the bubble layer thickness is of the same order as the height. The bubbles got squeezed down to the bottom, making the liquid supply from the leading edge difficult. At higher flow velocity inside the big channel, the second mechanism is becoming more and more important. However inside the 1.59 mm flow channel, the second mechanism disappeared, causing a relatively large CHF drop compared to the slow flow.

3.4.4 Effects of Heater Geometry

The in-line heater array has three heaters installed. The distance between the heaters can be varied. Experiments were conducted to find out the effects of other heaters on CHF. The following three charts indicate the typical results obtained from experiments with various distance between heaters.
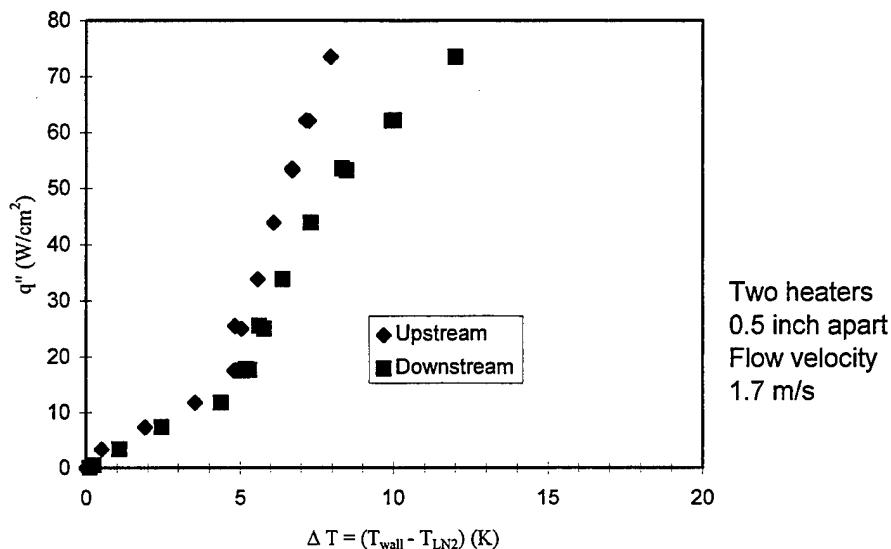
Figure 3. 9   Two Heaters with Distance of 0.5 Inch

Two heaters
1 inch apart
Flow velocity
0.8 m/s
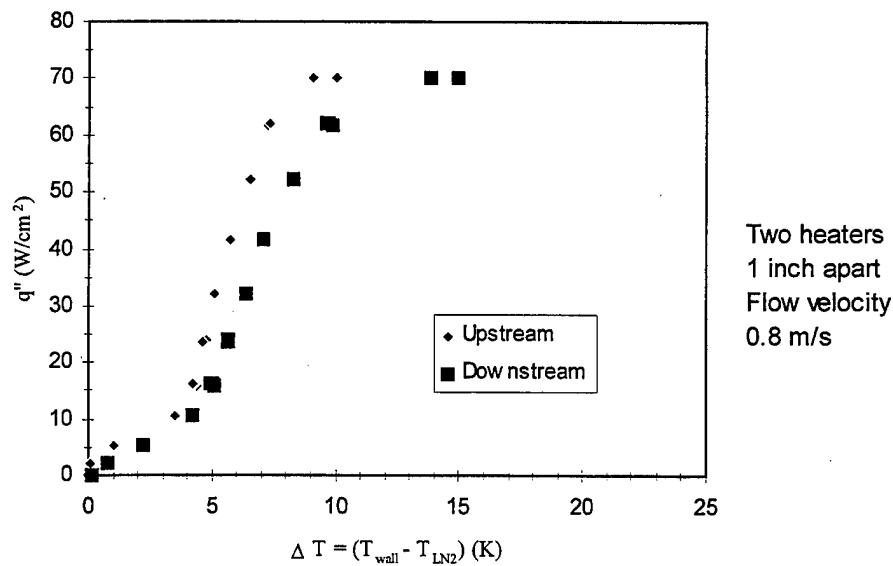
Figure 3.10   Two Heaters with Distance of 1.0 Inch

Two heaters
2.4 inches
apart
Flow velocity
2.0 m/s
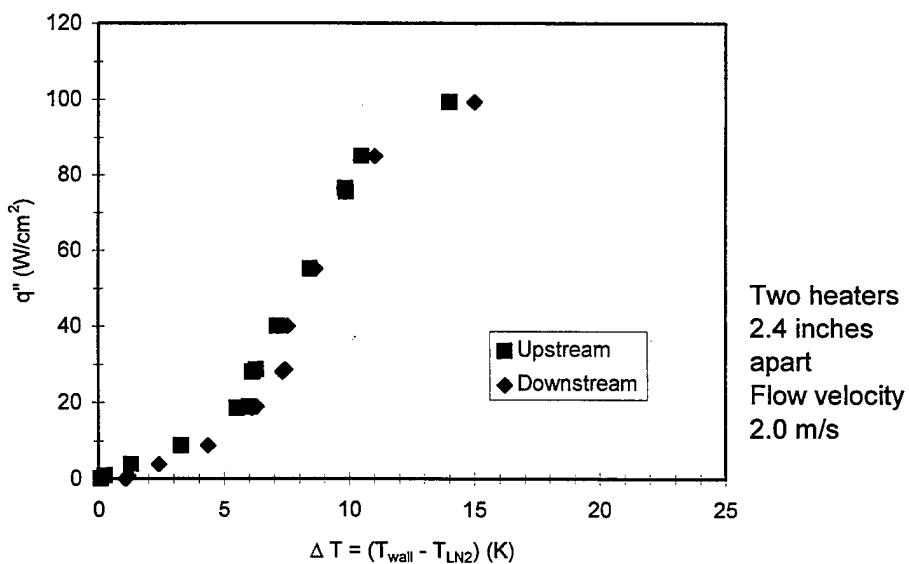
Figure 3.11   Two Heaters with Distance of 2.4 Inches

Two heaters were switched on. The distance between then was adjusted from 0.5 inch to
2.4 inches. When they were separated by 0.5 inch, the downstream heater reached CHF earlier

than the upstream one. From Figure 3.9, it can be seen that the two curves behaved differently. The upstream curve shifted to the left and still went up while the downstream curve already reached CHF. The liquid absorbed the heat from the upstream heater and vaporized. The bubble generated from this was pushed by the flow and flew over the second heater. The mixture two-phase flow made the heat transfer condition worse. The heat transfer coefficient obviously decreased. These bubbles also blocked the liquid supply to the heater which led to the early CHF. The CHF in Figure 3.9 was dropped by 20% or more. When the distance between the two heaters was increased to 1.0 inch, the two curves seemed to move closer to each other (Figure 3.10). The most important fact was that they were reaching CHF almost simultaneously. Figure 3.11 illustrated the result when the distance was reached 2.4 inches. The two heater behaved like similarly, as if the upstream heater had no effect on the second one. It gave the bubble enough space and time to float up to the upper section of the flow channel, and therefore, clear the way for liquid supply to the downstream heater.

It is then concluded that the distance between the chips is an important factor in electronic cooling applications. There exists a geometrical limitation for chips when they are packed in the electronic board. When they are too close to each other, the downstream chips will reach CHF and burn out while there still a lot of cooling potentials unused for the upstream chips.
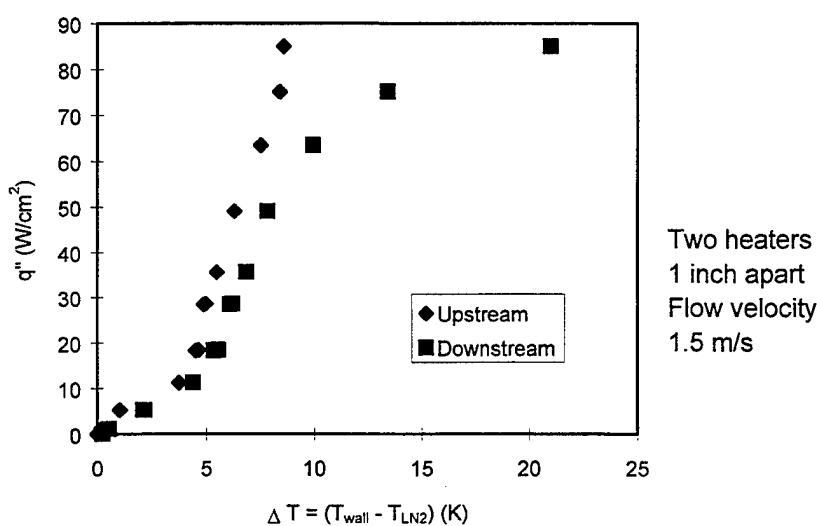
Figure 3.12   Two Heaters with Higher Velocity

46

Another important factor to be considered is the effect of flow velocity. Figure 3.12 shows that when the flow velocity increased from 0.8 m/s to 1.5 m/s, the downstream heater reached CHF before the upstream one. This is because when the liquid flow is slow, the bubbles generated from the upstream have enough time to float to the upper section of the flow channel, and therefore, having less effect on the downstream heater. The two heaters behaved more like single heater in the flow channel. When the flow velosity was high, the bubbles were pushed to the second downstream heater. They could not float up much, thus the void fraction of the liquid near the surface of the second heater was higher than the slow flow situation. Under this condition, the second heater reached CHF earlier than the first one.

3.5 Conclusions and Recommendations

In summary, the preceding sections discuss the effects of flow channel and chip geometries on CHF. These effects were obtained in conjunction with the effects of flow velocity so that a general map of CHF phenomena could be obtained. Knowledge of CHF is of paramount importance for the design and operation of electronic cooling schemes that employ any type of boiling heat transfer. A model was developed in this study to better understand and predict the CHF. Based on this model, flow boiling CHF can be accurately predicted over the range from 0.5 m/s to 2.0 m/s. For low and moderate turbulent flow situations, the thickness of macrolayer can be estimated.

Higher CHF could be achieved under higher flow velocity. Faster liquid flow improved the liquid supply condition and helped to remove the vapor bubbles. The heat transfer coefficient was also increased under the higher flow velocity due to the thin and constantly fed liquid macrolayer.

The effects of channel heights on CHF was small until it reached the same order as the bubble layer thickness. For a very small channel height, the decrease of CHF at lower flow

velocity was not as significant as that at higher flow velocity. It is because of the fact the two dominant factors which control the occurrence of CHF were not affected equally under the different flow velocity. It is recommended in electronic applications that electronic boards should be installed away from one another at least 1.59 mm.

When multiple chips were installed, the distance between the chips was a very important parameter to the system designer. It is recommended that the chips should be packed at least 0.5 inch apart at slow and moderate coolant flow velocity. At high flow velocity, the distance must be adjusted farther.

4.   MOSFET SIMULATION AND FABRICATION

4.1 Introduction

The main goal of the program is to explore the thermal management of high heat flux devices using cryogenic fluids. Cryogenic cooling is vital to high power applications used in many military systems. Such examples are solid-state R.F. amplifiers, hypercooling alternators, radar systems, and high-temperature superconducting hybrid power switches, capacitors, and inductors. The main emphasis of the project is to model, fabricate, and test power MOSFET's operating characteristics at cryogenic temperatures.

The development of the power MOSFET allows an electronic circuit designer greater flexibility in switching and power applications. This is due to 1) infinite input impedance, 2) zero output impedance, and 3) very fast on-off, with little or no switching losses. One of the more commonly used power MOSFETs is the double diffused vertical MOSFET (DMOS). For power applications this makes an excellent choice due to its short channel length, high breakdown voltage, and high current capabilities of the device. One aspect of the program is to fabricate a Power MOSFET in the lab and perform testing on it with LN2, and comparing the results to those at room temperature. The next phase of the project is to model and perform a simulation of the device using ISE-TCAD software and compare its characteristics to that of the real device previously fabricated.

4.2 Device Physics at Cryogenic Temperature

Despite the DMOS's short channel length, its breakdown voltage can be very high. This is due to the fact that the depletion region between the substrate and the body extends mostly in

the lightly doped substrate and does not spread into the channel (Figure 4.1). In the saturation region, drain current through the DMOS is equal to:

$$i_D = k \left(v_{GS} - v_T \right)^2 \tag{4.1}$$

$$\text{where} \quad k = 1/2 \, \mu_n \, C_{OX} \, (W/L) \tag{4.2}$$

where μ_n is the electron carrier mobility and L is the channel length of the device. As a result, increasing electron mobility and decreasing channel length will cause an increase in drain current.
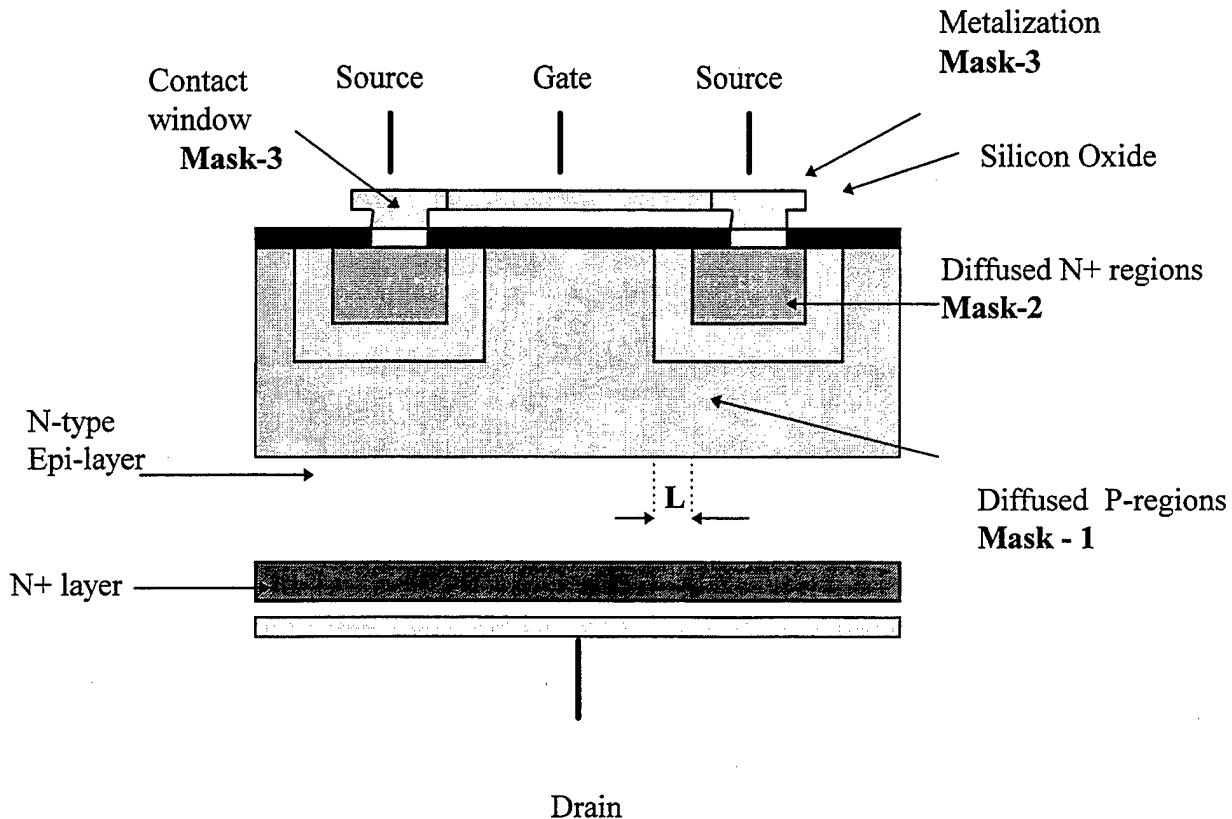
Figure 4.1 Cross Section of the Power MOSFET

Electron and hole mobility through a lattice structure are influenced by two basic types of scattering mechanisms: impurity scattering and lattice scattering. For temperatures greater than 50 K, carriers through the Silicon are scattered by the vibration of the lattice structure, also known as lattice scattering. In this temperature range mobility is proportional to $T^{-3/2}$. As

temperature decreases mobility will increase. As a result, majority carrier semiconductor devices such as MOSFETs will have a greater mobility at cryogenic temperatures as compared to room temperature [3]. Utilizing this effect, conductivity is directly proportional to mobility:

$$\sigma = qn\mu_n \qquad (4.3)$$

As a result of this phenomena, as mobility increases, conductivity (σ) will decrease. Also, this increase in mobility corresponds to an increase in saturation transconductance (g_m), and depending on the circuit application, an increase in switching speed and power dissipation.

4.3 Using ISE-TCAD Software For Device Simulations

It has been established that the operation of power MOSFETs at cryogenic temperatures will lower the overall resistance of the device as well as increase both electron mobility and the device's transconductance. With the ISE-TCAD software, the user can accurately model virtually any type of semiconductor device and analyze a number of parameters through a graphical interface. The user configures three main programs which instruct the ISE-TCAD software as to the type of device to be modeled, including its material composition, doping descriptions, and voltage and/or current ranges. The user also specifies the sequence of equation solving the software is to execute. The program has a default temperature range of 250 K to 500 K, however the user can enable a thermodynamic model which allows any temperature to be assigned to the device. This model also takes into account self heating effects of the device. This will be of great benefit when analyzing a power MOSFET at cryogenic temperatures.

The ISE-TCAD software is a computer aided design program that simulates virtually any semiconductor device's characteristics and operation. In order to accurately simulate a semiconductor device, the user develops the following three typewritten programs:

- The Boundary File
- The Command File
- The Input File

Once these files have been created the user then uses two internal files, M-Draw and Dessis, to perform the simulation which will be illustrated by Picasso and Inspect; both of which are

51

graphical interfaces to the software. M-Draw uses the Boundary and Command files to provide the physical parameters of the device to Picasso, while Dessis provides the computational information (i.e., how the device operates under certain conditions) to Picasso and Inspect. Picasso is an interactive visualization tool that utilizes the data from Dessis and M-Draw to develop high quality pictures of the simulated semiconductor device. Inspect is another graphical interface used to create graphs that the user defines for further parameter evaluation. The Boundary file is a typewritten C+ shell program composed by the user to define the physical dimensions of the semiconductor device to be simulated. These parameters include oxide layers, contacts, and the type of substrate used. In this file the user can assign virtually any commonly used substrate material such as silicon, polysilicon, or gallium arsenic, and any oxide layer such as silicon dioxide or silicon nitride.

The Command file is also a typewritten C+ shell program used to characterize the profiles of impurity distribution including concentrations, boundaries, and types of impurity used. In addition, the user can define an optional refinement area to be analyzed under tighter dimensions. An example of this is the case of a MOSFET where the channel length is typically a few angstroms thick. The Command file can also incorporate Gaussian profiles, error function profiles, constant function profiles, and lateral diffusion. The user can assign dose, standard deviations, and junction depth, to more accurately depict real life conditions of diffusion or ion implantation processes. The Input file consists of eight parts: Electrode, Thermode, File, Interface Conditions, Physics, Plotting, Math, and Solve. Of these, the main emphasis is on the last five listed.

- The Interface Conditions section is used to characterize interface charge conditions and recombination velocity. This is an optional section used for the insulation - substrate boundary of a device.

- The Physics section is used to describe physical models to be used in the simulation. Here we describe mobility modeling, incorporating such things as doping dependence, high field saturation, and electric fields. The user can also incorporate oxide charge, carrier to carrier scattering, and methods of recombination (including Shockley-Reed-Hall recombination, Auger recombination, and avalanche generation). Here the user also assigns one of the

following keywords: "temperature," "thermodynamic" or "hydrodynamic," which will be used in the Dessis program.

- The Plotting section is used to designate the variables that are to be solved for in both the Dessis program and can be observed visually by Picasso. Virtually any variable conceived by the semiconductor analysis can be observed including conduction current, hole and electron current/density, lattice temperature, electron and hole mobility, temperature, and lifetimes, electron and hole Joule temperature.

- The Math section is used to specify the numerical methods in order to solve Poisson's equation, Electron equation and Hole equation. The user specifies the number of Newtonian iterations that are to be used to solve the above equations until the error between the iterations (default is 10^{-3}) is achieved.

- The Solve section is used to specify what equations Dessis uses to solve and the method of solving. It is also used to describe a transient voltage condition or a quasi-stationary (ramping) voltage condition applied to a specified contact. Transient and quasi-stationary conditions can be evaluated for instance using a MOSFET device where the user can supply a constant gate voltage and vary the drain voltage to a specified value.

Once the Boundary, Command, and Input files have been established, the user then runs the program M-Draw. M-Draw creates a visual representation of the diffusion characteristics, physical boundary conditions, and a mesh profile of its Green points. All of these conditions can be edited by the M-Draw graphical interface. The Dessis program is then used to perform simulations based on Drift-diffusion, Thermodynamic and Hydrodynamic transport models. From the Solve section of the Input file, Dessis will solve the Poisson's equation, Electron current continuity equation, and Hole current continuity equation, using the fully coupled Newtonian method until the specified accuracy has been achieved. Poisson's equation is:

$$\nabla \bullet \varepsilon \nabla \psi = -q \, (p - n + N^+_D - N^-_A) \qquad (4.4)$$

where ε is the electric permitivity, q is the elementary electronic charge, n and p are the electron and hole densities, and N^+_D and N^-_A are the number of ionized donors and acceptors, respectively. The electron and hole continuity equations are as follows:

$$\nabla \bullet J_n = qR + q(\partial n / \partial t) \qquad (4.5)$$

$$-\nabla \bullet J_p = qR + q(\partial p / \partial t) \qquad (4.6)$$

where R is the net electron-hole recombination rate and J_n and J_p are the electron and hole current densities given by:

$$J_n = -nq\mu_n(\nabla\phi_n) \qquad (4.7)$$

$$J_p = -pq\mu_p(\nabla\phi_p) \qquad (4.8)$$

where ϕ_n and ϕ_p are electron and hole quasi-Fermi potentials.

In addition to using the standard Drift-diffusion model, Dessis can also account for self heating effects by the use of the Thermodynamic model. In this model, once the electrostatic potential and the electron and hole densities have been found, the amount of heat generated within the device is also determined. This model takes into account electrothermal effects under the assumption that the charge carriers are in thermal equilibrium with the lattice. Using this model, Dessis can evaluate electron and hole Joule heat, recombination heat, and Thomson heat. As a result, equations (7) and (8) will be modified to:

$$J_n = -nq\mu_n\,(\nabla\phi_n + P_n\nabla T) \qquad (4.9)$$

$$J_p = -pq\mu_p\,(\nabla\phi_p + P_p\nabla T) \qquad (4.10)$$

where P_n and P_p are the thermoelectric powers. Dessis uses a default temperature of 300 K. Simulations at uniform lattice temperatures between 250 K and 500 K are accurate with or without the Thermodynamic model incorporated.

After Dessis has solved Poisson's equation, Electron current continuity equation and Hole current continuity equation, a print out will be generated by the program to show electron, conduction, and hole currents over a specified range of voltages. Once the Dessis and M-Draw programs have been completed, the user can then execute Picasso-ISE.

4.4 Fabrication of the Power MOSFET

The design of the four layers of masking was performed using Auto-Cad. The masks were drawn originally on a 10x scale, then sent to a photo-reduction facility in order to produce a 10x reduction of each mask on an individual transparency. The next step then, is to transfer each of these masks onto a glass slide using photolithography. With the use of these glass slides, photolithography and thermal diffusion techniques will be used to fabricate the Power MOSFET

in the Fabrication Lab at the University of Central Florida. Figure 4.2 is the overhead view of each mask layer that will be used in the fabrication of the device, with the overall dimensions given. All dimensions are in units of microns. Again, referring to Figure 4.1 is the cross section of the Power MOSFET with the mask numbers shown, and the result of what each mask layer will ultimately produce. Initially, a dense layer of silicon oxide is grown on the silicon wafer. Mask-1 is to open the window in the silicon oxide for the P-type (boron) dopant to be diffused into the N-type silicon wafer. During the diffusion of the boron, silicon oxide will again grow on the wafer. Mask 2 is to open the window in the newly grown silicon oxide so that the highly doped N-type (phosphorus) can be diffused into the P-type boron well. Again, a layer of silicon oxide will grow on the surface of the wafer as a result of the previous diffusion process. Mask-3 will then open a window in the silicon oxide in preparation for the metalization so that the contacts can be produced. A thin film of aluminum will be deposited onto the wafer, and Mask-4 will then be to define where the etching of the unwanted aluminum is to be established. The masks also include the fabrication of the N and P type resistors, P-N and Schottky diodes. The extra devices in the mask will allow for easy measurements and characterization of the diffused materials in order to more accurately describe the parameters, such as doping concentrations, oxide thickness and metalization integrity of the device.
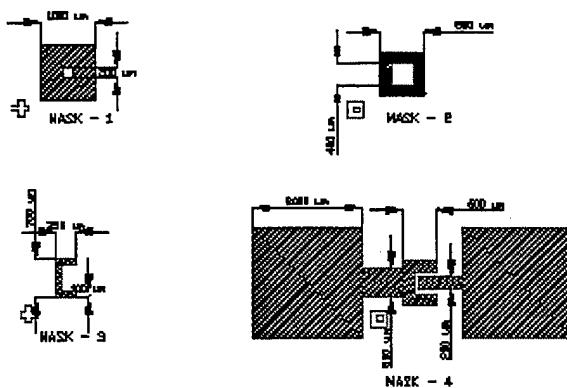

Figure 4.2   Masks

4.5 Derivation of the Diffusion Schedule

In order to achieve the proper dopant profile of the device, the following Diffusion Schedule for Boron is set (See Appendix 1 for a detailed derivation). Given the following: Background concentration of the N-type wafer $(N_b) = 1.5*10^{15}/cm^3$, Diffusion coefficient (D_O) of Boron of $10.5 cm^2/sec$. The Boron activation energy is 3.69 eV, and the predeposition of the Boron is to be performed at $900°$ C, for 600 seconds. Drive-in of the Boron is to be done at $1100°$ C, for 1800 seconds. The Solid Solubility of Boron at $900°$ C (N_{oB}) is $5.40*10^{20}/cm^3$, therefore yields the following results for the Boron Diffusion:

Boron Diffusion Schedule and junction depth results

Predep Temperature (°C)	Predep Time (seconds)	Drive-in Temperature (°C)	Drive-in Time (seconds)	Junction Depth (cm)
900	600	1100	1800	$1.492*10^{-4}$

As a result, the Boron will diffuse into the substrate as a Gaussian profile as exhibited in Figure 4.3. After the Boron is deposited into the wafer, the Phosphorus is now to be deposited where the diffusion coefficient (D_O) of Phosphorus of $10.5 cm^2/sec$. The Phosphorus activation energy is 3.69 eV, and the predeposition of the Phosphorus is to be performed at $950°$ C, for 600 seconds. Drive-in of the Phosphorus is to be done at $1100°$ C, for 600 seconds. The Solid Solubility of Boron at $950°$ C (N_oP) is $6.00*10^{20}/cm^3$, therefore yields the following results for the Phosphorus Diffusion:

Phosphorus Diffusion Schedule and junction depth results

Predep Temperature (°C)	Predep Time (seconds)	Drive-in Temperature (°C)	Drive-in Time (seconds)	Junction Depth (cm)
950	600	1100	600	$2.650*10^{-5}$

As a result, the Phosphorus will diffuse into the Boron wells to produce the Gaussian profile as seen in Figure 4.4.
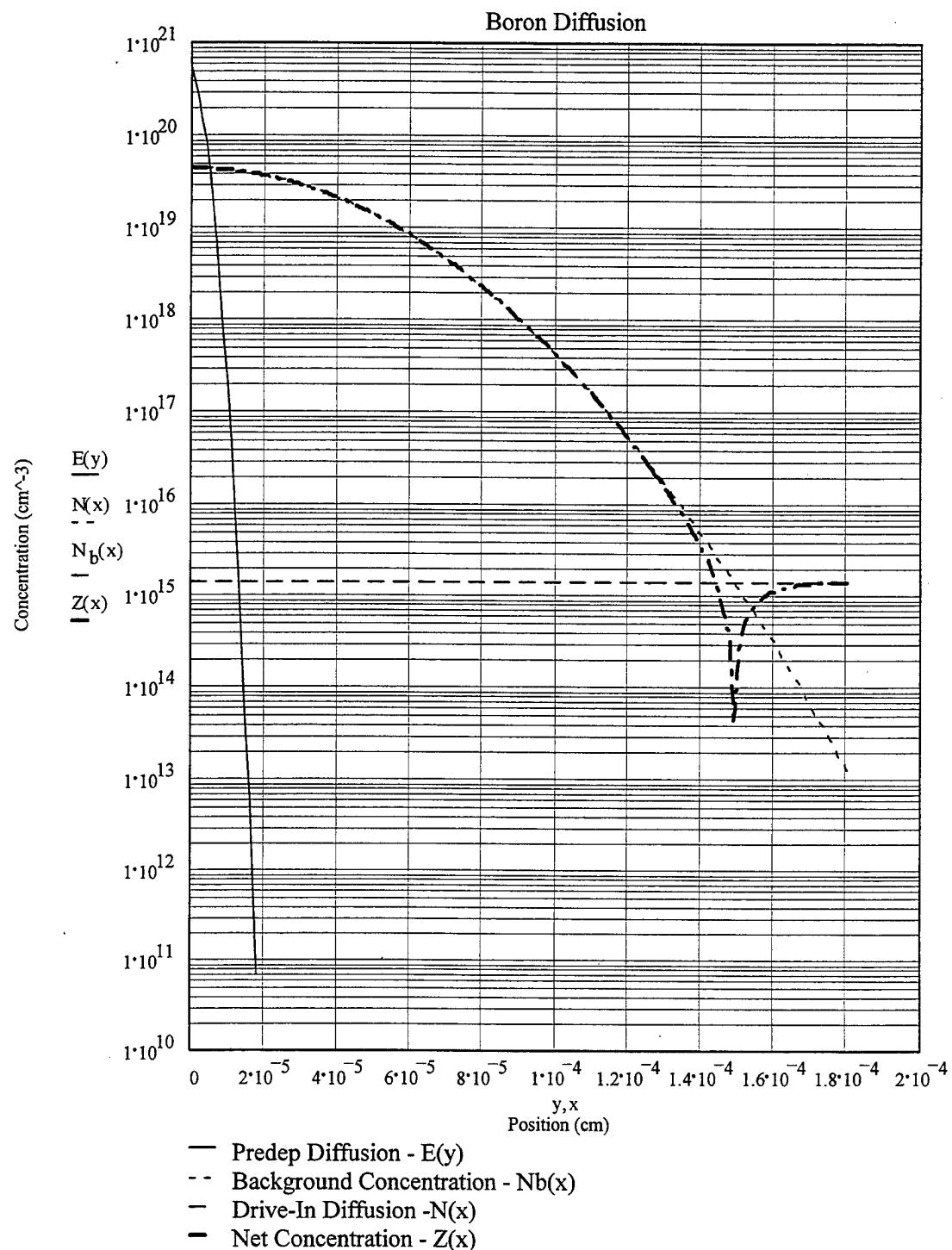
Figure 4.3 Graph of Boron Diffusion
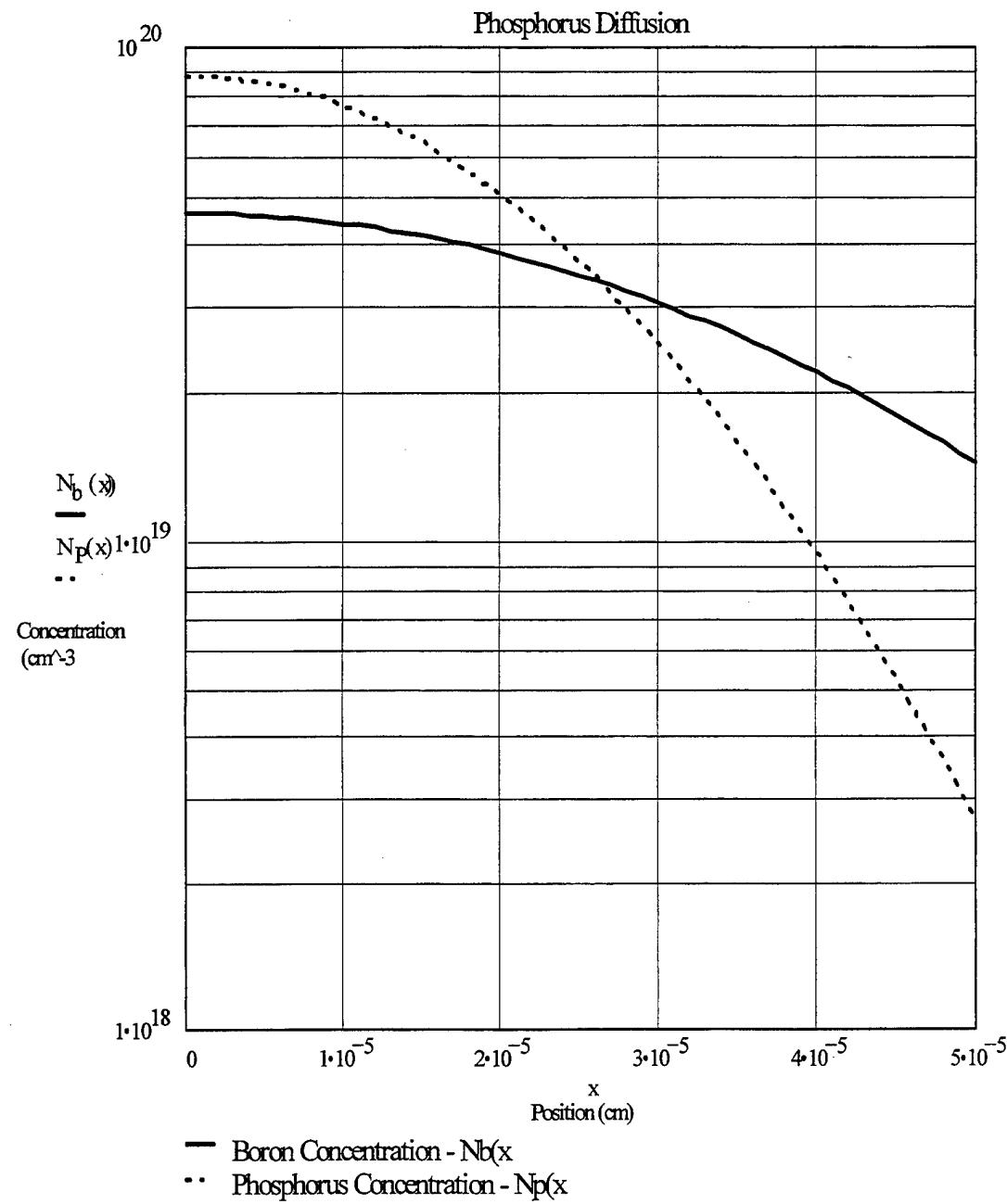
Figure 4.4 Graph of Phosphorus Diffusion

4.6 Conclusion

MOSFETs used in power applications can have power ratings of up to and exceeding 125 Watts. With such a small surface areas involved, power dissipation can be in excess of 200 W/cm^2. Previous research has determined that on-resistance decreases while mobility of the electrons increase while the Power MOSFETs is exposed to cryogenic temperatures. The fabrication of a Power MOSFET and the complete modeling and simulation of that device by the use of ISE-TCAD software will give an improved insight to the physics involved, and possibly even improved processes needed to design an even better device in the future. This aspect of the project will study the effects at room temperature and LN2 temperature, while ISE-TCAD simulations will also be done at 150 Kelvin as a prelude to even further research.

Appendix 4.1   Derivation of the Diffusion Profile

$D_o := 10.5$ $\qquad$ $T_1 := 950 + 273$ $\quad$ $E_a := 3.69$ $\qquad$ $k := 8.617 \cdot 10^{-5}$ $\quad$ $t_1 := 600$

$T_2 := 1100 + 273$ $\qquad$ $t_2 := 1800 \ sec$ $\quad$ $\dfrac{t_2}{60} = 30$ $\ min$ $\quad$ $N_b := 1.5 \cdot 10^{15}$

$D_1 := D_o \cdot \exp\left(-\dfrac{E_a}{k \cdot T_1}\right)$ $\qquad$ $D_1 = 6.527 \cdot 10^{-15}$

$D_2 := D_o \cdot \exp\left(-\dfrac{E_a}{k \cdot T_2}\right)$ $\qquad$ $D_2 = 2.992 \cdot 10^{-13}$

Solid Solubility of Boron at 900k : $\quad$ $N_{oB} := 5.400 \cdot 10^{20}$

The diffusion coefficient multiplied by time for predep (x1) : $\qquad$ $x_{1B} := t_1 \cdot D_1$

$\qquad$ $x_{1B} = 3.916 \cdot 10^{-12}$

The diffusion coefficient multiplied by time for drive-in (x2) : $x_{2B} := D_2 \cdot t_2$

$\qquad$ $x_{2B} = 5.386 \cdot 10^{-10}$

The Dose for Predeposition (Q): $\qquad$ $Q := 2 \cdot N_{oB} \cdot \sqrt{\dfrac{x_{1B}}{\pi}}$ $\qquad\qquad$ $Q = 1.206 \cdot 10^{15}$

The final surface concentration, (No): $\qquad$ $N_{0B} := \dfrac{Q}{2} \cdot \dfrac{1}{\sqrt{\dfrac{x_{2B}}{\pi}}}$ $\qquad\qquad$ $N_{0B} = 4.604 \cdot 10^{19}$

Junction Depth of the Boron Diffusion will be: $x_{jB} := 2 \cdot \sqrt{x_{2B} \cdot \ln\left(\dfrac{N_{0B}}{N_b}\right)} \cdot 10^4$ $\quad$ $x_{jB} = 1.492$ $\ um$

The constant profile of the background concentration is: $\qquad$ $N_b(x) := 1.5 \cdot 10^{15}$

And the error function profile of the predeposition is:
$$E(y) := \left(N_{oB}\right) \cdot \left(1 - \mathrm{erf}\left(\frac{y}{2 \cdot \sqrt{x_{1B}}}\right)\right)$$

The Gaussian distribution function is:
$$N(x) := \left(N_{0B}\right) \cdot \exp\left[-\left(\frac{x}{2 \cdot \sqrt{x_{2B}}}\right)^2\right]$$

The net profile at junction depth is:
$$Z(x) := \left| N(x) - N_b(x) \right|$$

See Figure 4.3 for the resultant profiles.

For the Phosphorus predeposition and Drive-in conditions :

$$D_o := 10.5 \qquad T_1 := 950 + 273 \quad E_a := 3.69 \qquad k := 8.617 \cdot 10^{-5} \quad t_1 := 600$$

$$T_2 := 1100 + 273 \quad t_2 := 600 \quad \sec \qquad \frac{t_1}{60} = 10 \quad \min \qquad \frac{t_2}{60} = 10 \quad \min$$

$$N_b := 1.5 \cdot 10^{15}$$

The solid solubility of Phosphorus at 950 C (Nop) : $N_{oP} := 6.00 \cdot 10^{20}$

The diffusion coefficient multiplied by time for predep (x1) : $\qquad x_{1P} := t_1 \cdot D_1$

$$x_{1P} = 3.916 \cdot 10^{-12}$$

The diffusion coefficient multiplied by time for drive-in (x2) : $x_{2P} := D_2 \cdot t_2 \quad x_{2P} = 1.795 \cdot 10^{-10}$

The Dose for Predeposition (Q): $\qquad Q := 2 \cdot N_{oP} \cdot \sqrt{\dfrac{x_{1P}}{\pi}} \qquad Q = 1.34 \cdot 10^{15}$

The final surface concentration, (Nop): $\qquad N_{0P} := \dfrac{Q}{2} \cdot \dfrac{1}{\sqrt{\dfrac{x_{2P}}{\pi}}} \qquad N_{0P} = 8.861 \cdot 10^{19}$

The equation for the Boron final Diffusion is: $\qquad N_b(x) := N_{0B} \cdot \exp\left[-\left(\dfrac{x}{2 \cdot \sqrt{x_{2B}}} \right)^2 \right]$

The equation for the Phosphorus final Diffusion is: $N_p(x) := N_{0P} \cdot \exp\left[-\left(\dfrac{x}{2 \cdot \sqrt{x_{2P}}} \right)^2 \right]$

The junction depth of the Phosousus Diffusion is where the two equations intersect (x) :

$x_j = 2.650 * 10^{-5}$ cm

See Figure 4.4 for the resultant profiles.

5. CONCLUSIONS AND RECOMMENDATIONS FOR FUTURE WORK

The experimental study of pool boiling is conducted to investigate the effects of heater angle orientation and confined spacing on boiling characteristics. In the open pool boiling, the horizontal upward-facing heater gives the highest CHF. Changes in CHF are not significant at $60°$ and $90°$ orientation. The downward-facing position causes the CHF to drop about 64% compared to the upward-facing position. Although at this orientation the CHF is the worst, the heat transfer coefficient saw an improvement. This is attributed to the thin layer of liquid that is produced between the heater surface and the bubbles. It is postulated that the buoyancy force pushes the bubbles against the heater surface squeezing the liquid macrolayer between the bubbles and the heater surface. It also slows down the vapor removal and liquid replenishing leading to a lower CHF.

The study finds a critical value (s=2.5mm) for the confined spacing. CHF decreases greatly as s is less than 2.5mm. The bubbles are thought to be deformed and moving closer to the surface due to the confined spacing. The heat transfer coefficient is higher also because of a thinner liquid sublayer.

For the heaters in an array, at the vertical orientation, the influence from the lower heater causes a lower CHF of the higher heater. How the induced convective flow would reduce the CHF of the upper heater will be continuously studied. The heater array in this stage of the experiment consists of three heaters. The heater base has the capability to study an array of nine heaters. The effect of multiple heaters on pool boiling in the main research objective of the next stage.

The forced convective boiling experimental apparatus is designed to allow visual observation of the phase-change phenomena of LN2 at the heat source. The effect of the LN2 flow velocity on the CHF has been studied. It has been shown that the thickness of the macrolayer beneath the vapor bubbles plays the most important role in determining the CHF. Experiments with different flow channel heights have been conducted. It is noted that the

channel height has little effect on the CHF until it is decreased to about the size of the vapor bubble layer. The experiment setup also allows an array of three in-line heaters. The dimensions of the heaters and the distances between the heaters are varied. The upstream heaters have a tremendous effect on heat transfer from the heaters located downstream. The two most important parameters in the multiple-heater situation are the distance between the heaters and the liquid flow velocity.

A model to describe the heat transfer mechanism near CHF is developed. A correlation was established using this model and the experimental data. This correlation provides an excellent fit to a wide range of experimental data.

As the CHF and the heat transfer coefficient are measured from the simulated chips, the experiment with MOSFET is prepared to obtain the operation characteristics of MOSFET in cryogenic temperatures. Both the pool boiling and the flow boiling steup can accommodate the MOSFET operation measurement without many modifications.

6. REFERENCES

1. Van Duzer, T. "Superconductor-Semiconductor Hybrid Devices, Circuits, and Systems," *Cryogenics*, Vol. 28 (1988), 527-531.

2. Mueller, O. M., "On-Resistence, Thermal Resistence and Reverse Recover Time of Power MOSFETs at 77K," *Cryogenics*, Vol. 29 (1989), 1006-1014.

3. Chui, C. J., Sehmbey, M. S., Chow, L. C., and Hahn, O. J., "Pool Boiling Heat Transfer from Vertical Heater Array in Liquid Nitrogen," *Journal of Thermophysics and Heat Transfer,* Vol. 9 (1995), 308-313.

4. Sehmbey, M. S., Chow, L. C., Hahn, O. J., and Pais, M., "Spray Cooling of Power Electronics at Cryogenic Tempreatures," *Journal of Thermophysics and Heat Transfer,* Vol. 9 (1995), 123-128.

5. Sehmbey, M. S., Chow, L. C., Hahn, O. J., and Pais, M., "Effects of Spray Characteristics on Spray Cooling with Liquid Nitrogen," *Journal of Thermophysics and Heat Transfer,* Vol. 9 (1995), 757-765.

6. Brusstar, M. J. and Merte Jr., H., "Effects of Buoyancy on the Critical Heat Flux in Forced Convection," *Journal of Thermophysics and Heat Transfer,* Vol. 8 (1994), 322-328.

7. Nguyen, D. N. T., "A Study to Determine the Effects of Heater Array Orientation and Confined Spacing in Liquid Nitrogen Pool Boiling," MS Thesis, University of Central Florida,   Orlando, FL, 1997.

8. Incropea, F.P., "Convective Heat Transfer in Electronic Equipment Cooling," ASME *Journal of Heat Transfer*, Vol. 110, No. 4, 1988, pp. 1097-1111.

9. Bar-Cohen, A., "Thermal Management of Air- and Liquid-Cooled Multichip Modules," *IEEE Transactions on Components, Hybrids, and Manufacturing Technology*, Vol. CHMT-10, No. 2, 1987, pp. 159-175.

10. Chu, R.C., "Heat Transfer in Electronic Systems," *Proceedings of the Eighth*

International Heat Transfer Conference, Vol. 1, August 1986, pp. 293-305.

11.   Nakayama, W. and Bergle, A.E., "Cooling Electronic Equipment: Past, Present and

       Future," *The International Symposium on Heat Transfer in Electronic and*

       Microelectronic Equipment, ICHMT, Dubrovnik, Yugoslavia, August 29-September 2,

       1988, pp. 1-37.

12.   Antonetii V.W., Oktay, S. And Simons, R.E., "Heat Transfer in Electronic Packages,"

       Microelectronics Packaging Handbook, Tummala, R.R., and Rymaszewski, E.J. Van

       Notrand Reinhold, New York, 1989, p. 168.

13.   Baker, E., "Liquid Immersion Cooling of Small Electronic Devices," *Microelectronics*

       and Reliability, Vol. 12, 1972, pp. 163-173.

14.   Hwang, U.P., and Morgan, K.P., "Boiling Heat Transfer of Silicon Integrated Circuit

       Chip Mounted On a Substrate," *Heat Transfer in Electronic Equipment*, Vol. 20, 1981,

       pp. 53-59.

15.   Megerlin, F.E. and Vingerhoet, P., "Thermal Control of Densely Packaged

       Microelectronics in Dielectric Fluids," NAECON' 71 Record, pp. 254-259.

16.   Baker, E., Liquid Cooling of Microelectronic Devices by Free and Forced Convection,"

       Microelectronics and Reliability, Vol. 11, 1972, pp. 213-222.

17.   McGillis, W.R., and Carey, V.P., "Immersion Cooling of an Array of Heated Dissipating

       Elements-An Assessment of Different Flow Boiling Methodologies," *Proceedings of*

       AIAA/ASME Thermophysics and Heat Transfer Conference, June 1990, Seattle, WA.

18.   Gunther, F.C., "Photographic Study of Surface-boiling Heat Transfer to Water with

Forced Convection," *Trans. ASME* 73, 1951, pp. 115-123.

19.   Galloway, J.E., and Mudawar, I., "CHF Mechanism in Flow Boiling from a Heated

Wall," *International Journal of Heat and Mass Transfer*, Vol. 36, No. 10, 1993,

pp. 2511-2526.

20.   Gersey, C.O., and Muddawar, I., "Orientation Effects on Critical Heat Flux from

Discrete In-line Heat Sources in a Flow Channel," *Journal of Heat Transfer*, Vol. 115,

1993, pp. 973-985.

21.   Leland, J.E., and Chow, L.C., "Forced Convective Boiling from a Nonflush Simulated

Electronic Chip," *Journal of Thermophysics and Heat Transfer*, Vol. 7, No. 4, 1993, pp.

588-594.

22.   Haramura, Y., and Katto, Y., "A New Hydrodynamic Model of Critical Heat Flux,

Applicable Widely to Both Pool and Forced Convective Boiling on Submerged Bodies in

Saturated Liquids," *International Journal of Heat and Mass Transfer*, Vol. 26, No. 3,

1983.

23.   Zuber, N., "On the Stability of Boiling Heat Transfer," *Trans. of ASME*, Vol. 80, 1958.

24.   Mudawwar, I., and Maddox, D.E., "Critical Heat Flux in Subcooled Flow Boiling of

Fluorocarbon Liquid on a Simulated Electronic Chip in a Vertical Rectangular Channel,"

International Journal of Heat and Mass Transfer, Vol. 32, No. 2.